Cellulose Nanocrystal Hybrids as Reinforcing and Antibacterial Agents in Rubber Nanocomposites

by
Joanna Jardin

A thesis

presented to the University of Waterloo

in fulfillment of the

thesis requirement for the degree of

Master of Applied Science

in

Chemical Engineering

Waterloo, Ontario, Canada, 2020

AUTHOR'S DECLARATION

I hereby declare that I am the sole author of this thesis. This is a true copy of the thesis, including any required final revisions, as accepted by my examiners.

I understand that my thesis may be made electronically available to the public.

ABSTRACT

As environmental consciousness increases and fossil fuel feedstocks are depleted, ecofriendly product development is of utmost importance. This thesis describes an in-depth analysis of cellulose nanocrystals (CNC) used as a promising nanofiller derived from cellulosic biomass. Pristine CNC, as well as CNC modified with tannic acid (TA) and silver (Ag) were investigated for reinforcing thin rubber sheets and films. Since polymers are major contributors to waste problems, the work conducted in these projects used natural rubber (NR) as a renewable polymeric material and compared it to synthetic rubbers, styrene butadiene rubber (SBR) and acrylonitrile butadiene rubber (NBR).

In the first part of the project, casted thin sheets of NR and SBR were tested and compared. Percolation of CNC was studied within the rubber matrices, where the tear strength, water permeability, and water absorption increased due to the formation of a continuous network of CNC within the polymer sheets. The rubber nanocomposites were resistant to tear propagation due to increased tortuosity along the tear path brought about by CNC dispersion and the continuous filler network. The CNC reinforcement yielded thin sheets that were stronger and more durable than their non-reinforced counterparts. Additionally, the increased water uptake of the sheets could aid in the biodegradation of the polymer. Thus, CNC was found to be an excellent functional filler in rubber sheets, where its formation of a percolating network significantly improved their properties.

Since CNC was found to be a useful thin film filler material, it was modified into CNC-TA-Ag to carry silver nanoparticles for antimicrobial functionality. Green chemical processes were used to deposit TA and Ag onto CNC, and optimized to achieve the highest silver nanoparticle content on the CNC. Successful material synthesis was confirmed by Transmission

Electron Microscopy (TEM), thermogravimetric analysis (TGA), and Ultraviolet-Visible Spectroscopy (UV-vis) analyses. The CNC-TA-Ag was proven to be effective against both Gram-negative and Gram-positive strains of bacteria, *E. coli* and *S. aureus,* respectively. A particular affinity was noted against *E. coli*, where only 3.2 μg silver/mL was required to completely inhibit microbial growth. Compared to reported literature studies, it was extremely effective against the bacteria, which is likely due to the capability of CNC to stabilize silver nanoparticles in aqueous dispersions. The CNC-TA-Ag was then incorporated into NR and NBR dipped films to emulate the mass production of thin film products. Mechanical tests revealed that CNC-TA-Ag increased the modulus of the rubber nanocomposite films, and effectively increased the tear strength. Preliminary antimicrobial tests showed a promising effect of the CNC-TA-Ag against bacteria when incorporated into neat NR. Based on these results, CNC-TA-Ag may be a useful filler for rubber thin film products, such as sterile antimicrobial gloves. The CNC-TA-Ag filler may also be extended for use in various other polymers or fibres to prepare self-sterilizing coatings and surfaces, paints, packaging materials, bandages, or adhesive nanocomposites.

ACKNOWLEDGEMENTS

I would like to express my sincere gratitude toward my two supervisors, Prof. Michael Tam and Prof. Tizazu Mekonnen, for the opportunity to pursue my interests in research. Thank you for your continuous support, expertise, and guidance in navigating the world of academia, and for the wisdom regarding various aspects of life. My supervisors have always had their doors open for discussion, and I have learned many things from them that will stay with me throughout my career.

I would also like to gratefully recognize Prof. Bill Anderson for his knowledge in antimicrobials, and for allowing us the use of his lab for bacterial testing. Thank you to the NSERC Tri-Agency scholarship for providing funding for this project as well. This research would not have gone as far without their important contributions.

My deepest thanks go out to Emmanuel Ogunsona, Ewomazino Ojogbo, Malin Ly, and Prachi Panchal – my wonderful officemates and friends. Thank you for all your help throughout our time together, both technically and mentally. I will never forget the friendship, food, and laughter that we all shared. I would also like to thank all members of Tam Group and Mekonnen Group for their kindness over the past two years. I have been surrounded by very talented people that have motivated me to strive for greatness.

I am extremely grateful for my family and close friends, who have always been there for me despite the physical distance between us. Thank you for keeping me positive and confident in myself; you have brought out the best in me. Life has taken us in very different directions, and I appreciate the fresh new perspectives you all bring to the table. Our experiences may vary greatly, but the bond we share has become stronger than ever. A special thanks to Tamzeed Mahdood, who

has been my beacon of calm and happiness. I cannot begin to express my appreciation for all the love and inspiration you have given me throughout the years.

Finally, a big thank you to all the committee members, Dr. Michael Tam, Dr. Tizazu Mekonnen, Dr. Xianshe Feng, and Dr. Evelyn Yim for their time in reading my thesis and providing insightful feedback. Your advice and commentary are greatly appreciated.

TABLE OF CONTENTS

LIST OF FIGURES

LIST OF TABLES

LIST OF ABBREVIATIONS

Ag	Silver
ASTM	American Society for Testing and Materials
CFU	Colony forming unit
CNC	Cellulose nanocrystals
CNF	Cellulose nanofibres
CNT	Carbon nanotube
COS	Chitosan oligosaccharide
DMA	Dynamic mechanical analysis
ENR	Epoxidized natural rubber
GO	Graphene oxide
GPE	Grape pomace extract
MIC	Minimum inhibitory concentration
MR	Molar ratio
NP	Nanoparticle
NR	Natural rubber
NBR	Nitrile butadiene rubber
PD	Polydopamine
PHB	Polyhydroxybutyrate
PLA	Polylactic acid
S	Sulfur
SBR	Styrene butadiene rubber
SEM	Scanning electron microscopy
TA	Tannic acid
TEM	Transmission electron microscopy
TGA	Thermogravimetric analysis
UV	Ultraviolet
WVT	Water vapour transmission
ZDBC	Zinc dibutyl dithiocarbamide
ZnO	Zinc oxide

CHAPTER 1

Introduction

1.1 The Importance of Renewable Materials

Polymers obtained from renewable resources have been accessible for many years, finding many valuable applications as naturally occurring high molecular weight macromolecules. In the early days of polymer science, the majority of materials were exclusively based on chemically modified biopolymers such as silk, natural rubber, casein, and ivory[1,2]. In fact, polymer development at the beginning of the 20th century was aimed at imitating these natural polymeric materials for their attractive properties[3]. After the discovery of macromolecular chemistry and polymerization by Hermann Staudinger[3], many advancements have been made in the field of polymer chemistry and engineering, leading to the production of fully synthetic polymers often obtained from the processing of petrochemical resources. These polymers can be produced to meet specific design criteria, such as enhanced thermal resistance, water resistance, mechanical strength, and processability. Synthetic polymers are now widely available for applications in packaging, electronics, automotive, and medical industries.

Synthetic polymers have been extremely useful; however, the problems with synthetic polymers have been amplified in recent years as environmental consciousness increases. One concern is the potential depletion of petrochemical feedstocks, as limited fossil fuel supplies may be exhausted within the next hundred years[4]. Another major issue is environmental pollution and its effect on natural ecosystems. It is estimated that approximately 6.3 billion tons of plastic waste was generated by 2015[5]. Of this amount, 79% was accumulated in landfills or in natural landscapes worldwide[5,6], and plastic waste continues to contaminate various areas of the planet. Microplastics have even been found in areas extremely isolated from human influence, such as the Mariana's Trench and other deep sea ecosystems[7].

There are many sources of polymer waste, some of which are unavoidable in the current state of technology. For example, 27 million scrap tires are annually disposed in landfills[8] despite tire recycling and reuse projects. Tires are primarily composed of styrene butadiene rubber (SBR) and, due to their dark colour from carbon black filler, exhibit excellent heat retention. This results in hazards from potential tire fires that generate toxic oils and smoke. Another leading example of polymer waste contributors are excessive medical wastes from hospitals. Several kilograms of disposable sterile items, such as gloves, syringes, and catheters are thrown into landfill daily. Gloves in particular make up the majority of laboratory waste, often made from nitrile rubber (NBR). Both SBR and NBR are non-biodegradable polymers and can take several thousand years to naturally break down on their own.

Although these synthetic elastomers require extreme heat and stress to degrade, they have an environmentally-friendly counterpart: natural rubber (NR). Natural rubber is an organically obtained latex, commercially harvested from the sap of *Hevea brasiliensis* trees[9]. NR has very versatile mechanical properties, and can be broken down by many microorganisms such as *Gordonia polyisoprenivorans, Streptomyces,* and *Thermomonospora* strains of bacteria[10]. Vulcanized natural rubber can also be biodegraded (but at a slower rate), or composted. Since recent research has moved back to the investigation of renewable polymers derived from feedstock such as biomass, it is of interest to explore natural rubber for more commercial applications. The goal is to address the concerns of pollution and sustainability, and create innovative functional materials that are not dangerous to the environment.

1.2 Research Objectives

The research conducted in this thesis studied the reinforcement of natural rubber with natural nanofillers compared to synthetic elastomers. The overall goal of the project was to produce elastomeric nanocomposites from renewable resources, and investigate a green polymer filler for advanced applications.

The first section of this thesis explored the enhancement of the mechanical properties of NR and SBR using cellulose nanocrystals (CNC). CNC is an ecofriendly filler and can potentially replace other harmful reinforcing additives in rubber products. Nanocomposite thin sheets were prepared with low and high loading levels of CNC, and they were studied for their morphology and physical properties. The effect of filler percolation on the mechanical strength, tear resistance, and water absorption properties was examined. The objective was to evaluate the viability of CNC as a sustainable reinforcing filler for use in common elastomeric materials.

The second section of this thesis focused on a multifunctional nanocomposite made of NR and chemically modified CNC. This nanocomposite used CNC as a carrier for antimicrobial silver nanoparticles, imparting both strength and antimicrobial properties to the rubber films. The successful optimization of silver nanoparticle growth on CNC was a key factor, using green synthesis methods. NR nanocomposite films were then prepared in a dipping process simulating industrial rubber glove production techniques. NBR nanocomposite films were also produced, as NBR is a commonly used glove material. The end goal of this project was to produce working film formulations for antimicrobial rubber, comparing both natural and synthetic latex. This material could have potential applications for surgical gloves, antibacterial condoms, or food packaging

handlers to reduce the risk of bacterial cross-contamination. The produced nanocomposite aims to outperform traditionally-used glove materials in three distinct ways: the NR product will be fully ecofriendly, exhibit antimicrobial activity, and have improved mechanical properties using less material. Overall, the applications of this research are widespread: a sustainable, antibacterial latex with excellent properties will benefit both humans and the environment alike.

1.3 Thesis Outline

This thesis is composed of five chapters. The first chapter presents the general motivation and objectives behind this research work. The second chapter reviews some literature to describe the current state of the field, including discussion on renewable polymer and filler materials with the focus on natural rubber and cellulose nanocrystals. Chapter two will also cover metal nanoparticles as antimicrobial materials, and antimicrobial composites. Chapter three describes the study of CNC used as a sustainable filler in NR and SBR thin sheets. The modification of CNC with silver nanoparticles is then covered in chapter four, corresponding to the preparation and analysis of antimicrobial film nanocomposites. Finally, the last chapter summarizes some conclusions from this work, and presents the future outlook for ecofriendly nanocomposite materials.

CHAPTER 2

Literature review

2.1 Renewable Polymers

There are many useful bioderived polymers, but in the current environment very few are commercially successful. In 2014, for example, more than 300 megatonnes of polymers were produced globally and merely 1.7 megatonnes of this value consisted of bioderived polymers[11]. The lack of renewable polymers in use can be attributed to the abundance of synthetic materials that boast a wide range of application-specific properties. Material selection in industrial production also leans towards synthetic materials due to their lower cost. Moving forward, a combination of environmental awareness and government policy can incite the adoption of more sustainable polymers to address global pollution problems.

Some common renewable polymers that have wide industrial potential include cellulose, starch, natural rubber (NR), polylactic acid (PLA), and polyhydroxybutyrate (PHB). General properties of these polymers can be found in Table 1 below.

Table 1: General mechanical properties of various renewable polymers. Data compiled from the Polymer Data Handbook[12].

Polymer	Tensile Strength (MPa)	Young's Modulus (MPa)	Glass Transition Temp (K)	Melting Temp (K)
Starch	35-46	--	496	460
Cellulose	100-1000	4000 - 108000	523 (thermal decomposition)	493-513 (start of thermal degradation)
Natural rubber	17-25	1.0 -2.0	201-212	313
Polylactic acid	28-50	1200-16000	323-337	418-459
Polyhydroxybutyrate	20-60	700-4000	268-278	320-453

As seen in the table, the base properties of these natural polymers are not as wide-ranging compared to the characteristics that can be obtained from synthetic polymers. The next step is therefore for researchers to find ways to improve these base properties.

2.1.1 Natural Rubber

As aforementioned, natural rubber is an environmentally-friendly counterpart to SBR and NBR and will be of primary focus in this thesis. Natural rubber is a good choice for replacing synthetic elastomeric materials since it is acquired from rubber trees. The structure of NR is composed of a repeat unit of isoprene (C_5H_8), as per Figure 1. NR obtained from plants contains C_5H_8 units with one double bond in the *cis* configuration; thus, NR is also referred to as poly(*cis*-1,4-isoprene). Latex from *H. brasiliensis* also has two *trans*-isoprene units in the terminal regions[10].

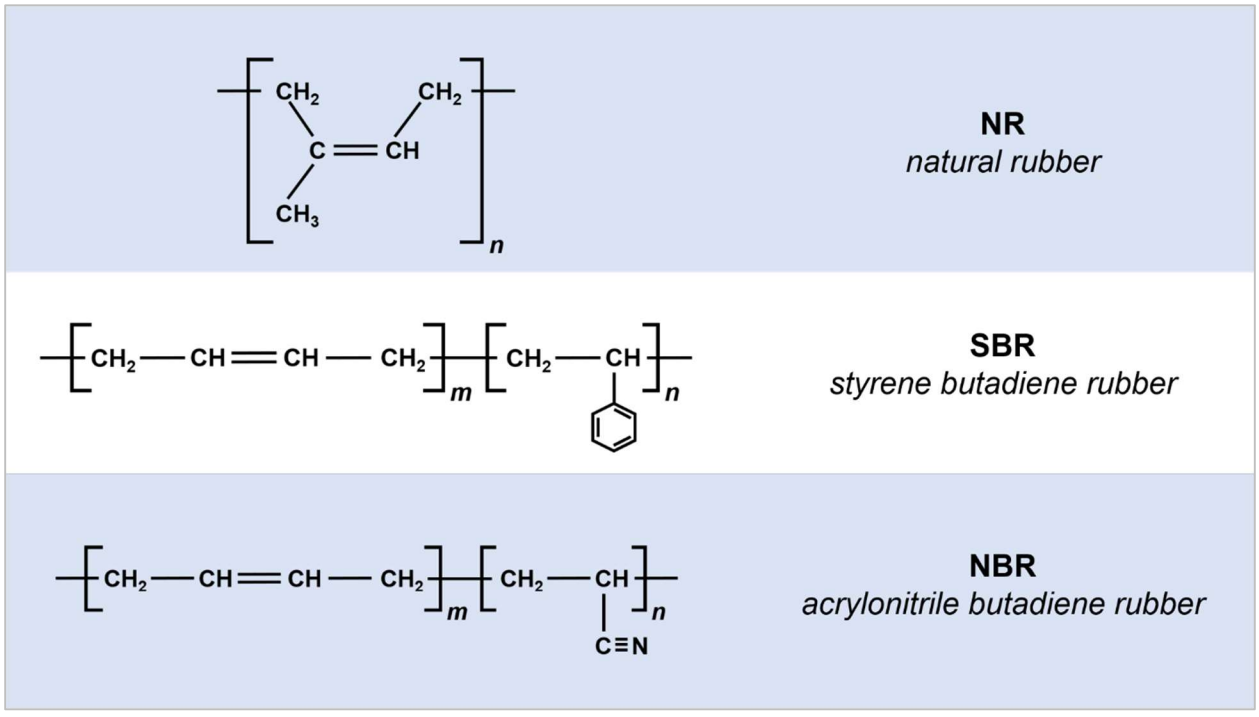

Figure 1: Chemical structure of natural rubber, styrene butadiene rubber, and nitrile rubber.

Although almost 2000 types of plants synthesize poly(*cis*-1,4-isoprene), only NR latex harvested from *H. brasiliensis* trees is produced commercially[10]. Latex is tapped from a mature tree, yielding 100-200 mL of latex resin within 3 hours. This can result in up to 2500 kg of natural rubber per year per hectare. NR can also be made synthetically through an emulsion polymerization reaction, which is referred to as "synthetic natural rubber".

NR resin in its neat form is obtained as a latex dispersion, and naturally contains about 30% poly(*cis*-1,4-isoprene). "Latex" refers to a stable colloidal emulsion of polymeric particles in aqueous medium[13]. The rubber particles are present in the form of 3-5 μm particles, and the rest of the dispersion is 50 to 70% (wt/wt) water[10]. There is also a small percentage (≤ 6%) of other particles such as proteins, lipids, and sugars[14] naturally present in the mixture. The proteins and lipids in NR latex act as natural surfactants, allowing for stabilization of the rubber particles[15] as depicted in Figure 2.

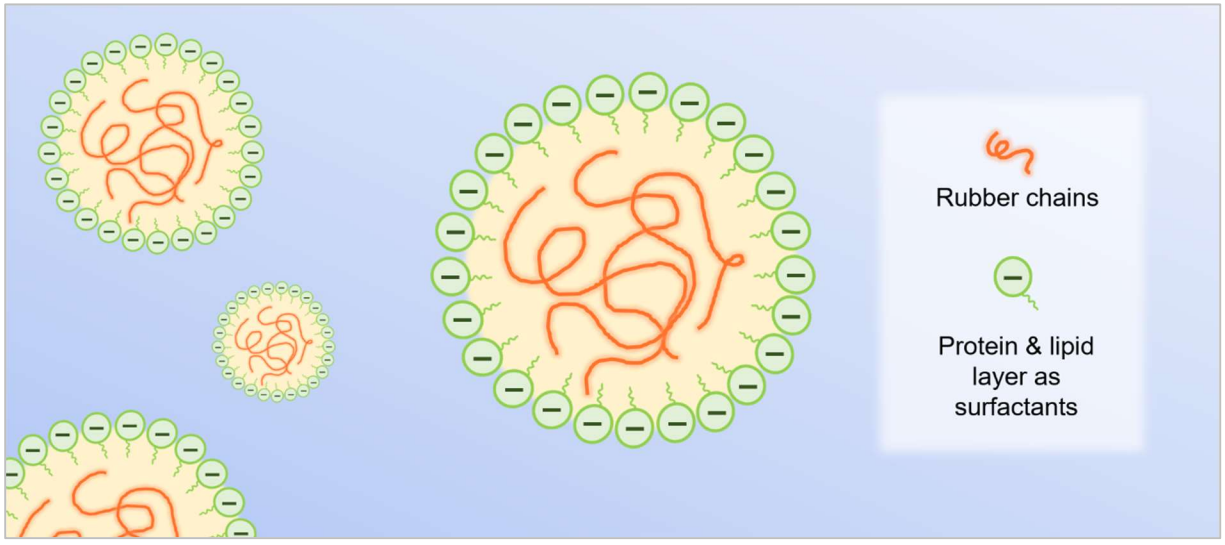

Figure 2: Rubber latex particles stabilized in an aqueous dispersion.

2.2 Rubber Processing

In order to obtain useful goods from rubber, it is distributed to manufacturing industries in a concentrated liquid latex form or as dried solid sheets. The four steps to process rubber include compounding, mixing, shaping, and vulcanization to create a final product.

Compounding involves the addition of compounds to the rubber that will allow for ease of processing and ensure the rubber has suitable properties. Reinforcing fillers, cross-linkers, plasticizers, and pigments are added to rubber during compounding, which is then followed by mixing to thoroughly disperse these additives. Some traditional additives will be discussed in detail in the following section. Shaping of the rubber is then performed. Techniques such as extrusion, coating, casting, or molding are implemented to shape the rubber into the desired form. Finally, the vulcanization step concludes the process by inducing chemical cross-linking to set the shape of the rubber.

2.2.1 Compounding and Mixing Additives

Traditional Structural Additives

Structural additives are necessary for the improvement of neat rubber properties. The most important structural additives for rubber are those that are involved in the vulcanization and curing processes, as curing creates more durable rubber. Most often, sulfur (S) or a sulfur donor is the favoured crosslinking agent for rubbers as it forms sulfur bridges between the polymer chains to create a three dimensional network from the linear polymer[16]. The mechanism of crosslinking involves the attack of the double bonds of neighbouring polyisoprene molecules, producing covalently bonded networks out of the polymer chains[16] as shown in Figure 3a. The activation

energy for the vulcanization of rubber by sulfur (33-36 kcal·mol^{-1}) is very similar to the bond dissociation energies for S-S bonds in molecular sulfur (33 kcal·mol^{-1}) and polysulfides (37 kcal·mol^{-1})[16].

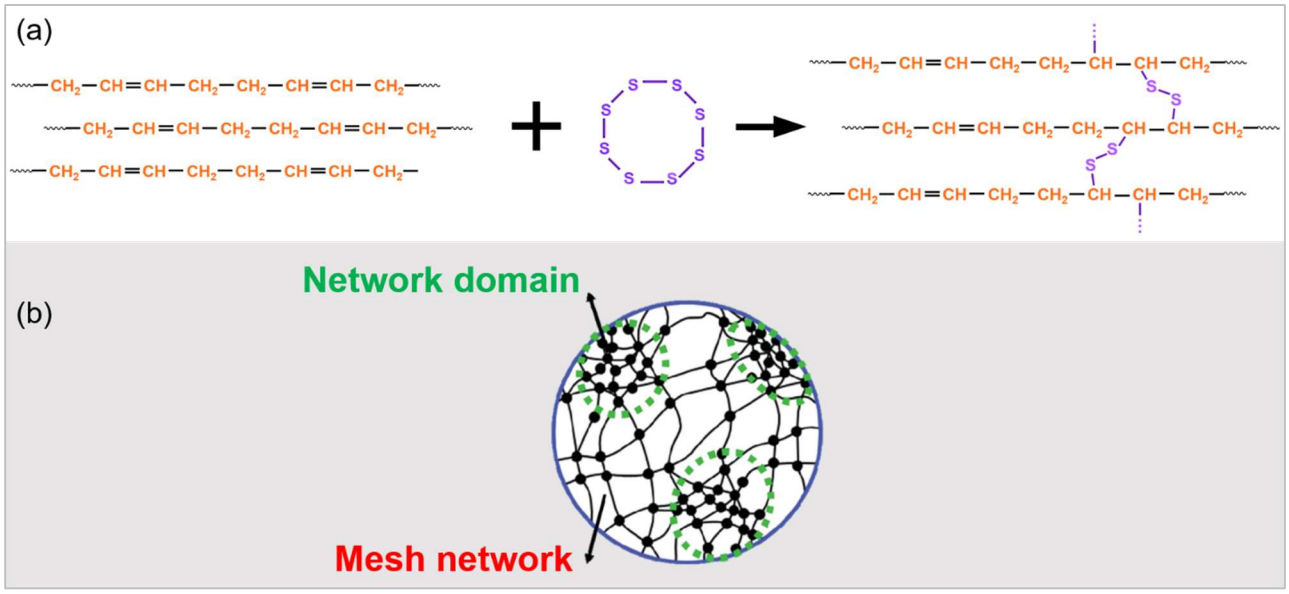

Figure 3: (a) Crosslinking of natural rubber, where sulfur attacks the double bond of polymer chains to attach chains to one another. (b) A two-phase rubber network is obtained after sulfur crosslinking[17].

Crosslinking via sulfur alone is a fairly slow process, and takes several hours at elevated temperature[16]. Activators and accelerators can therefore be used to achieve crosslinking in periods within the range of a few minutes. Common accelerator types include guanidines, dithiocarbamates, thiophosphates, thiazoles, and sulfonamides which are effective catalysts for the crosslinking reaction[16]. Typically, zinc oxide (ZnO) is used as an activator[18], along with stearic acid as a surfactant to solubilize the ZnO. The activator facilitates the opening of elemental sulfur rings to form polysulfide ions, then zinc sulfide is produced as a reaction intermediate[16]. Due to the complicated chemical reactions between rubber, sulfur, and many other crosslinking reagents

involved, an exact mechanism of accelerated vulcanization has still not been conclusively defined[16,17,19].

A recent study by Yasuda et al. has further characterized the physical structures obtained from ZnO-activated sulfur vulcanization. It has been found that there is inhomogeneity in the structural networks formed during isoprene crosslinking. A two-phase network containing a mesh network and network domains with highly branched areas was characterized using X-ray absorption fine structure (XAFS) spectroscopy during vulcanization at 140 °C (Figure 3b)[17]. The formation of the mesh network was observed to progress earlier than that of the network domains[17]. This may suggest a phenomena between ZnO and the stearic acid surfactant that requires further investigation.

Traditional Functional Additives

Functional additives are those that impart an additional feature to the polymer, rather than merely being necessities for processing and structural integrity. The most common functional additive used in the rubber industry is carbon black. Carbon black is produced through the incomplete combustion of heavy petroleum products, and is a major additive used in NR and SBR tires for reinforcement and pigment. It is also a long-term and low-cost UV absorber, primarily effective by absorbing UV rays and transforming them into heat which is dissipated throughout the polymer. Carbon black also provides UV protection through an antioxidant effect via free radical scavenging, and catalytic decomposition of peroxides[20]. It contains many stable radicals that are able to scavenge for reactive species and prevent polymer chain scission[21].

Carbon black particles can range from a few nm to 500 nm in size, depending on the mechanism of generation[22]. Smaller particles have been shown to be more effective as UV absorbers, due to the increased surface area available for UV absorption and blocking as well as better dispersion[20,22]. Small sizes are also ideal as they show a delay in the loss of ultimate elongation of polymers compared to larger particle fillers[20]. However, use of carbon black is being limited in recent products as it is potentially carcinogenic, and it is obtained from depleting fossil fuel sources that create harmful greenhouse gas emissions during production.

Other nanomaterials have also emerged as useful functional additives and will be discussed in further sections. Due to their small surface area to volume ratio, nanoparticles are ideal functional additives because they can achieve a similar effect to their micron-sized counterparts at much lower loading levels[23]. That is, their size allows for better dispersion and distribution throughout a polymer matrix and thus leads to higher reinforcement. Regular structural additives can also be chemically modified to create functional additives and serve multipurpose goals.

2.2.2 Latex Shaping and Vulcanization

Once additives have been mixed into latex, the transformation of a stable colloidal dispersion of polymer particles into a continuous film is called "latex film formation"[13]. This is part of the shaping process of rubber. Films and thin sheets of rubber can be formed in two ways: through casting or dipping. These processes will be discussed in detail below.

Casting

Casting is the process of pouring liquid latex into a mold, often made from plaster, and allowing the latex to dry until a solid film is produced. As water evaporates, a concentrated dispersion of

rubber transforms into a packed array of particles, which then forms a solid polymer film upon removal of all moisture. The process can be split into three steps: drying, particle deformation, and diffusion[13]. Often, these steps may overlap in time, and they are illustrated in Figure 4.

As NR latex dries, isoprene molecules get closer together and one molecule attacks the carbon-carbon double bond of another molecule. This initiates the polymerization process and breaks the double bond in the molecule. More active sites are then created, eventually forming long chains of isoprene molecules: polyisoprene. The polyisoprene strands then form electrostatic bonds with one another, holding the rubber fibres together to create the final latex film. This process of drying NR is then completed by curing, heating the NR to elevated temperature to encourage cross-linking of the polymer chains.

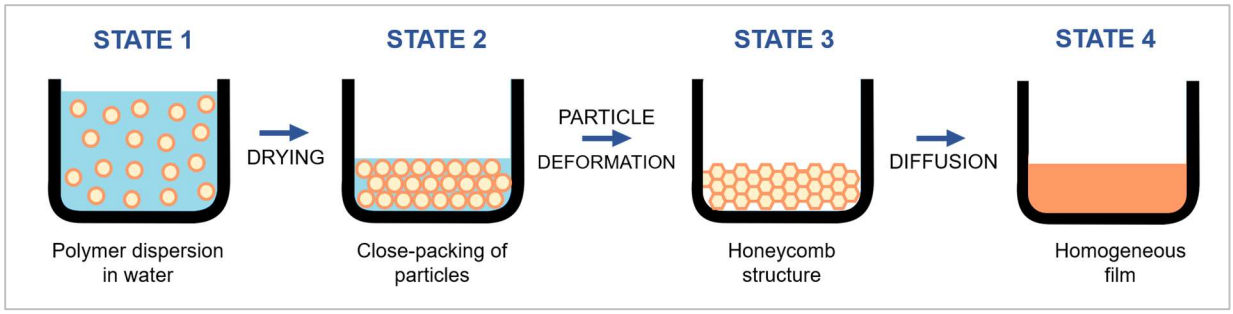

Figure 4: Casting and drying process to form a continuous polymer film. Adapted from [13].

Dipping

Dipping involves shaping the latex onto the surface of a former. Often the former is made from glass or ceramic and is shaped in the form of the desired product; for example balloons, gloves, or condoms. To start the process, the former is dipped into a coagulant mixture. Coagulant primarily consists of calcium nitrate and calcium carbonate in aqueous solution. These ingredients are dried to form a layer on the former, then the former is dipped into a pre-cured latex mixture. Nitrate ions

from the coagulant act to destabilize the polymer particles to adhere to the former surface. The latex-dipped product is then placed in an oven for drying and curing of the film. This allows the rubber to set and maintain its shape. Due to the directional movement of dipping, the process may create an alignment of filler additives in the matrix. An anisotropic material can then be produced, enhancing properties in a particular direction.

2.3 Emerging Nano-Additives

In recent years, many advances in the polymer field have taken advantage of the use of nano-sized additives. Nanomaterials are generally defined as having at least one dimension that is < 100 nm in size. Due to the extremely small size of nanoparticles and their ability to interact with polymer chains on a molecular scale, nanocomposites may have properties (or a combination of properties) that cannot be obtained in the bulk polymer or in conventional macro- or micro-composites[24]. In the current state of research, ingredients such as nanosilica, nanoclay, graphene oxide, carbon nanotubes, magnetite, chitin, and cellulose nanomaterials are being thoroughly investigated in various rubber substrates.

Nanosilica particles (SiO_2) have become particularly important in tire applications since the introduction of the Green Tire by Michelin[25]. Compared to carbon black, silica has greater reinforcement power for improving tear strength, abrasion resistance, age resistance, and adhesion properties[25]. However, silica-filled rubbers and carbon black-filled rubbers both exhibit a Payne effect which can cause rolling resistance in tire applications. The Payne effect refers to the pronounced decrease in the storage modulus of highly filled rubbers with increasing strain amplitude under cyclic loading[26]. This effect is related to either the rubber-filler or filler-filler

interactions, where the existing microstructure is altered with recurring application of force. A study by Meera et al. investigated silica nanoparticles in NR substrates[27]. It was found that a larger Payne effect exists due to stronger filler-filler networks that can be formed because of the small particle size and high specific surface area of nanosilica[27]. The current trend is therefore to mix various fillers in order to interrupt the particle-particle interactions and minimize Payne effect.

Nanoclay is another reinforcing filler that has been researched in rubber nanocomposites. Nanoclays are layered mineral silicates, including classes such as montmorillonite, bentonite, kaolinite, and halloysite. They are non-toxic with a layered structure that can achieve different morphology within polymer matrices: intercalated or exfoliated configurations. Intercalated structure involves the insertion of polymer chains within the layered clay structure, whereas exfoliated morphology destroys the layered configuration of the nanoclay and clay platelets are distributed throughout the composite. Studies by Praveen et al. and Qu et al. combine traditional carbon black filler with varying concentrations of nanoclay in SBR and NR, respectively[28,29]. Intercalated clay structures with some exfoliation were visible through TEM micrographs. Both groups found a synergistic effect between the carbon black and nanoclay, resulting in higher tensile strength for rubber containing both fillers. This could allow for at least partial replacement of carbon black with nanoclay in industrial production, while simultaneously improving the composite properties.

Graphene oxide (GO) can be used in rubber for supercapacitor applications, and carbon nanotubes (CNTs) can be used for piezoresistive sensor nanocomposites[30–33]. GO and CNTs are widely used in electronics, both containing sp^2 hybridized carbon. In CNTs, this creates a high degree of electrical conductivity as each carbon contains one free electron, which is easily

delocalized within the CNT structure to conduct electricity. Meanwhile, GO with low degree of oxidation can act as a semiconductor, or as an insulator with full degree of oxidation[34]. Suriani et al. showed composites of NR-GO exemplified good capacitive behaviour under an applied voltage, thus demonstrating potential use in energy storage devices[30]. Similarly, multiwalled CNTs were investigated by Selvan et al. in NR nanocomposites for piezoresistive sensor applications. Piezoresistive material resistance changes upon deformation, thus they can be used as electrical sensors to monitor stresses and mechanical damages[33]. Because of the high aspect ratio of CNT, they were shown to percolate in the host NR. Strongly non-linear resistance behaviour was then observed as a function of strain. This material could be used as a strain sensor due to its flexibility, ease of manufacturing, and sensitivity[33].

From these examples, it is clear that there are many types of nano-additives that have shown promise in various rubbers for the production of useful materials. Nano-additives will likely play a large role in product development in the future as research advances. These nano-sized materials and nanocomposites are excellent additives, whether they are simply for reinforcement and improved mechanical properties, or for specialty applications to create conductive rubber, sensors, or other multifunctional products.

2.4 Cellulose Nanomaterials

In this thesis, cellulose nanomaterials have been chosen as the nanomaterial additive of focus due to the many advantages they offer. Though it has been demonstrated that there are many useful nano-sized compounds, cellulose nanomaterials are of significant interest since cellulose is produced in mass quantities through nature, is non-toxic, and biodegradable[35]. These properties

have become a major attraction as industries and academia both shift focus into sustainability, recycling, and environmentally-friendly product development.

First and foremost, cellulose nanomaterials can be synthesized from many types of agro-wastes[35–37]. From wood pulp, sugarcane bagasse, cotton, bamboo, and other plant-based material waste, the production of cellulose nanomaterials provides a useful way to recycle these scrap components. The manufacturing process begins with cellulosic biomass, consisting of high molecular weight chains of β-1,4-linked D-glucose units. Cellulose is the most abundant polymer found in nature, as it is a major component of plant cell walls used for maintaining structure. The linear cellulose chains hydrogen bond with one another to form microfibrils, which contain both crystalline and amorphous regions. Thousands of hydrogen bonds between cellulose molecules create a very stable and strong complex with high strength.

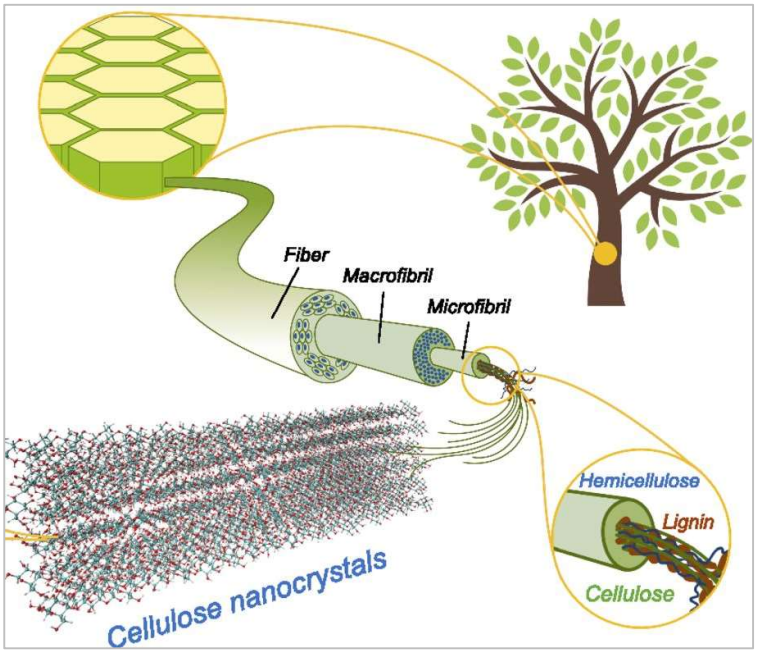

Figure 5: Cellulose nanocrystals obtained from the hierarchical structure from plant cell walls[38].

To produce nanocrystals from the cellulose, acid hydrolysis is performed, and most often sulfuric acid or hydrochloric acid is used. During this reaction, the acid cleaves bonds in the amorphous region of the cellulose microfibrils due to the disordered structure and the greater spacing between chains. Closely-packed crystalline regions are less susceptible to attack. Through control of the reaction time, highly crystalline cellulose nanocrystals (CNC) can be obtained (Figure 5). Longer cellulose nanofibers (CNF) can also be manufactured from cellulose, requiring mechanical processes such as homogenization or grinding to break down cellulose chains into fibrous nanosized threads. Of these two cellulose-based nanomaterials, CNC will be the main compound of study in this work.

The high crystallinity of CNC leads to excellent physical properties. Dimensions of individual CNC can range from 2-50 nm in width and 100-2000 nm in length[39], thus they have a high aspect ratio. Due to their small size and low density, the surface area per volume of CNC is 150-250 $m^2 \cdot g^{-1}$. In terms of mechanical properties, they exhibit an elastic modulus from 110-220 GPa and tensile strength of 7.5-7.7 GPa[39,40]. This indicates that CNC can be an effective reinforcing agent in composite materials.

The structure of CNC contains many hydroxyl (-OH) groups, many of which are available for modification on the CNC surface. Sulfuric acid hydrolysis introduces additional sulfate esters to the CNC surface to enhance colloidal stability. Meanwhile, hydrochloric acid cleaving imparts minimal surface charge to the CNC while preserving the large quantity of reactive hydroxyl groups in the structure. Overall, the hydroxyl-rich surface lends CNC a high potential for modifications: oxidation, esterification, etherfication, silyation, or polymer grafting can be performed to achieve additional properties.

The large-scale production of CNC has been achieved by several companies, including CelluForce Inc. and FPInnovations in Canada. The CNC can be distributed in either gel suspension or powdered forms. CelluForce produces CNC with a capacity of 1 tonne/day[41], a significant production volume considering the nano-size of CNC. This bulk production makes CNC easily accessible for study in many applications, and feasible for use in commercial products. It is therefore useful to encourage CNC use in existing and new formulations.

2.4.1 Cellulose Nanocrystals for Reinforcement

Due to its robust mechanical properties, CNC can be used directly as a polymer additive for reinforcement. For example, Chen et al. explored the reinforcement of foamed NBR with CNC[42]. Rubber foams are used as lightweight damping materials that absorb vibration and allow for thermal or acoustic insulation. Since pure rubbers are unable to provide sufficient mechanical properties, they are often reinforced with inorganic fillers[42]. CNC can provide an attractive environmentally friendly alternative for strengthening the foam properties. In their study, CNC had a diameter of approximately 100 nm and a length around 500 nm. It was found that the CNC greatly enhanced the foam tensile strength and elastic modulus, and also increased the rate of NBR curing. Overall, there was a strong interaction between the CNC and NBR matrix which allowed for smaller foam sizes and therefore better mechanical properties.

CNC in both NR and epoxidized NR (ENR) was studied by Tian et al. for tunable water-responsive behaviour[43]. In this study, nanocomposite films were prepared by casting NR and ENR with CNC loading levels of 1, 3, 6, and 10%. Water responsiveness was tested using dynamic mechanical analysis (DMA), and it was found that the ENR composites showed better water sensitivity than the NR composites. ENR contains epoxy groups in its structure, which impart

additional sites for hydrogen bonding with the CNC filler. This allowed for enhanced filler dispersion and a dual network between filler-filler and filler-polymer that resulted in stronger adaptive mechanical properties upon exposure to water. Films with the highest CNC loading were seen to demonstrate the greatest change in storage modulus after immersion in water. After redrying, both NR and ENR composite films were able to recover their maximum storage modulus values. Interestingly, the ENR composites with CNC had a higher storage modulus after redrying than the initial readings, likely due to a more favourable reorganization of the CNC network in ENR after redrying[43]. This recoverable water-responsive property could be useful in biomedical applications.

Barrier applications are also important properties in thin films, and Dhar et al. studied the effect of CNC on the gas barrier characteristics of poly-3-hydroxybutyrate (PHB)[44]. As PHB is a biodegradable polymer, the nanocomposites could be promising replacements as food packaging materials. In this study, CNC (with a diameter of 15-20 nm, and length of 400-600 nm) were synthesized from bamboo pulp and incorporated into PHB at loading levels of 1, 2, 3, and 5 wt%. Even at low loading, the PHB-CNC films showed a significant decrease in the oxygen transmission rate through the composite material. At 1 and 2 wt% CNC loading, the oxygen transmission rates decreased by 45.7 and 64.5%, respectively. This improvement can be attributed to the hydrogen bonding between CNC and the hydroxyl groups on PHB, as well as the increased tortuosity in the films which resisted the diffusion of oxygen molecules. The enhanced gas barrier could be particularly useful for foods that require preservation in an inert gas environment.

From these CNC-reinforced nanocomposites, it has been proven that CNC can be a useful filler with many advantages for creating stronger and versatile polymer products. Potentially, these

advantageous properties of CNC can benefit thin film products by facilitating the production of thinner films with high toughness and barrier properties, allowing manufacturers to save on costs during production. Since CNC is also sustainable and biodegradable, it could prove to be a very valuable commodity as industries address the demand for green goods.

2.4.1 Cellulose Nanocrystals for Medical Use

On their own, the properties of CNC are already very promising as a rigid strengthening filler. Upon chemical modification, however, an even more versatile CNC nanomaterial can be created. Modified CNC often have dual utility as a reinforcing agent and also imparting specialized functionalities to a nanocomposite. The hydroxyl-rich surface of CNC make it easy to introduce other chemical species for an additional range of capabilities. Some examples of CNC modification for composites include applications such as: hydrophobic surfaces, UV protection, magnetic properties, water treatment, and electronics[45–49].[18]

With the wide variety of fields that can benefit from the use of modified CNC, modifications for medical use are particularly appealing. CNC that are able to effectively kill bacteria are useful for creating sterile surfaces, preventing infections, and protecting workers in the healthcare industry. CNC can also be modified to carry drugs and other materials on its surface.

Antibacterial CNC

The preparation of antibacterial CNC is useful for self-sterilizing surfaces in the medical field. Research on the modification of CNC for the purpose of inhibiting bacteria is therefore gaining traction. An example of antibacterial CNC is the grafting of rosin to the surface of CNC, as studied by de Castro et al[50]. Rosin is a product of pine trees, and is a known antibacterial[51]. In their project,

CNC was chemically modified to carry rosin using green synthesis methods through esterification at 130 °C for 10 hours. The final rosin-CNC was effective as an antibacterial against Gram-positive bacteria, specifically *B. subtilis*. A weaker but still observable activity was noted against Gram-negative bacteria (*E. coli*), hence this research opens opportunities for rosin-CNC use in functional surfaces.

Yu et al. synthesized antibacterial CNC through the introduction of zinc oxide (ZnO) to the CNC surface[52]. ZnO nanoparticles (NPs) have been studied to partially dissolute and release Zn^{2+} ions that exhibit antimicrobial activity against strains of both bacteria and fungi[53]. To synthesize the ZnO-CNC, Fischer esterification was performed on CNC to impart carboxyl groups to its structure. Zinc nitrate hexahydrate was then added to the CNC to form $Zn(OH)_2$-CNC via electrostatic interactions. Upon heating at 120 °C, the $Zn(OH)_2$ was transformed to ZnO to form the final ZnO-CNC material. Antibacterial tests indicated that the ZnO was able to inhibit the growth of both *S. aureus* and *E. coli*, whereas the CNC did not show any antibacterial activity on its own. The size of ZnO was observed to play a significant role in bacterial inhibition, where smaller ZnO NPs (42.6 nm average diameter) on the CNC were more effective than larger ZnO NPs (126.6 nm and 143.1 nm average diameter).

A more common metal for antimicrobial purposes is silver (Ag). In a study by Shi et al., silver NPs were anchored to the surface of CNC using dopamine[54]. Dopamine was first reacted with CNC to result in polydopamine (PD)-CNC, then they were added to a silver nitrate solution. Dopamine hydrochloride was used as a reducing agent for silver ions to form nanoparticles and create the resultant Ag-PD-CNC. Compared to a dispersion of free Ag NPs, the Ag-PD-CNC dispersions were proven to be much more stable over a period of 3 months. As metal nanoparticles

have a high surface energy, they tend to aggregate in solution; however, the CNC effectively stabilized the NPs and prevented this. Antibacterial tests using the modified CNC showed excellent antibacterial properties, inhibiting 99% of bacterial growth at concentrations of 4 and 8 μg/mL against *E. coli* and *B. subtilis*, respectively. This activity was four times more effective than free Ag NPs, thus the CNC was proven to be a very effective carrier material.

These results show that modified CNC are very versatile carriers for antibacterial agents, and are beneficial as stabilizing substrates to prevent aggregation of high surface energy particles. Metal nanoparticles such as zinc and silver can greatly benefit from attachment to CNC. This research will further the use of CNC for stability of metal nanoparticles using green synthesis methods.

2.5 Metal Nanoparticles

Metal NPs have emerged as popular bactericidal materials within the past decade. Overuse and misuse have caused antibiotics to become less effective, as bacteria adapt to antibiotics with mutations[55]. Metals are therefore gaining traction as antibacterial alternatives. Different metals have long been known to possess antibacterial properties: for example, silver vessels were used in ancient Greece to prevent spoilage of liquids; gold foil has been used in dental inlays to inhibit bacterial infections; and copper door handles and surfaces are known to self-disinfect due to the oligodynamic effect[56–58]. Nanoparticles of these different metals have therefore been created and tested to assess their potential as treatments for bacterial infections. In particular, silver is the most popular metal NP for antibacterial treatments as it is highly effective at low concentrations, and has low toxicity at these exposure levels.

2.5.1 Silver Nanoparticle Synthesis

In order to form silver NPs, a top-down or bottom-up approach can be implemented as depicted in Figure 6[59]. Top-down approaches begin with bulk material, which is then mechanically or chemically broken down into nano-sized particles. This includes techniques such as mechanical milling, laser ablation, etching, or sputtering techniques[60]. In contrast, bottom-up approaches begin with simpler atoms or molecules that are assembled to construct NPs. Often, a bottom-up approach in solution is performed. This method is less costly and requires less energy input than a top-down approach, and provides the ability to better control particle size[61,62]. Using bottom-up techniques, metal molecules in solution must cluster to create small units that make up the nanoparticle. Upon synthesis, metal nanoparticles often have very spherical shapes with narrow size distribution [63]. Other forms such as triangular, hexagonal plates, or rod-like configurations are also possible with adjustments in pH, molar ratios, and temperature to induce slower reactions and therefore encourage anisotropic growth into desired shapes[64].

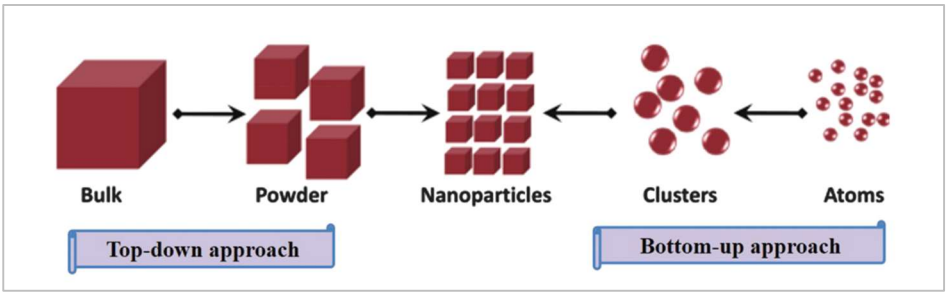

Figure 6: Top-down approach (left to center) compared to bottom-up approach (right to center) methods of producing metal nanoparticles[59].

There are three basic requirements for the bottom-up synthesis of silver NPs: a metal precursor, a reducing agent, and a capping agent. The synthesis process typically begins with a metal precursor such as silver nitrate ($AgNO_3$) that solubilizes well in aqueous solution to yield an

abundance of Ag^+ ions. A reducing agent that can easily donate electrons, such as sodium borohydride, is then added to the solution to create Ag^0 ions[62,65,66]. The Ag^0 and Ag^+ ions combine together into small clusters as they begin to nucleate. Coalescence of several nuclei form the final Ag NP spheres. A capping agent is then added to stabilize the particles in solution and stop growth. By controlling the reaction time, amount of reducing agent, and type of capping agent, the size of the Ag NPs can effectively be controlled[66].

2.5.2 Mechanism of Antimicrobial Activity

The mechanism through which silver nanoparticles act as effective bactericides has not been fully studied nor understood, but there are several proposed hypotheses. In order to fatally damage bacteria, Ag NPs may act against microbes both externally and internally, by inducing physiochemical changes to the cell wall or through the disruption of several internal biological functions.

The first proposed mechanism of antibacterial action suggests that electrostatic interactions exist between positively charged silver ions and the negatively charged cell membranes of microorganisms[67,68]. These interactions allow Ag NPs to attach themselves to the bacteria cell wall, where the silver ions act to modify the cell membrane proteins and affect the phospholipid bilayer[69,70]. This results in irreversible damage to the cell, such as increased membrane permeability and subsequent leakage of intracellular fluids. Li et al. previously observed this through fragmented areas and pits in bacterial cell walls upon SEM and TEM imaging of silver-nanoparticle-treated strains[71]. Direct damage to the cell wall can also aid in penetration of metal ions to the inside of the bacterium.

The second proposed mechanism speculates that metal ion dissolution from the nanoparticles interact with proteins and other integral components within the cell. Once ions have entered a bacterium, these ions can react with sulphur-containing compounds, inducing the inactivation of vital proteins[72]. Ions may also interact with phosphorous-containing compounds such as DNA, preventing successful replication and subsequently cell replication through binary fission[72]. Metal ions therefore play a significant role in interrupting key intracellular functions.

Finally, the third mechanism indicates that reactive oxygen species (ROS) generation is brought about by metal nanoparticles. The nanoparticles can supply a sustained release of metal ions within the cell due to the lower pH[73]. These ions react to create free radicals, such as superoxide ions, hydrogen peroxide, and hydroxyl radicals. Due to the excess of ROS, the cell is unable to attain homeostasis or mount an effective antioxidant response; thus inducing oxidative stress and resulting in cell death.

Likely, the actual mechanism of action of silver nanoparticles is a combination of these proposed mechanisms, but further study is required. Silver nanoparticles have consistently proven their effectiveness against various bacterial strains. Due to their extremely large surface area to volume ratio, NPs allow for much better contact with bacteria compared to their larger-sized metal counterparts[74]. Additionally, Ag NPs may employ several approaches against bacteria that are the key difference that drive them above traditional antibiotics.

2.6 Antibacterial Nanocomposites

The addition of silver nanoparticles or antimicrobial-modified-CNC to a polymeric matrix can create functional antibacterial nanocomposites. These can be extremely useful in healthcare, for

use during medical procedures, or in post-treatment. Sterile environments are also a necessity in food production and packaging industries, thus antibacterial polymer materials are a highly valuable advancement for many fields.

2.6.1 Wound Dressing Nanocomposites

One application of silver NPs in medicine is in bandages and wound dressings. An example of a commercially available product containing Ag NPs is PolyMem Silver®, a polyurethane (PU) foam nanocomposite containing starch used for burn dressings[75]. Many dressings rely on silver NPs to easily produce silver ions due to their high surface area to volume ratio[76]. The high surface energy of silver NPs can cause them to aggregate, thus forming on a polymer or fiber is ideal to keep them stable. Silver NPs can be added to textiles or polymers to form nanocomposites in two ways: either through forming Ag NPs directly on the fiber surface, or by adding pre-synthesized Ag NPs to the fiber material (as seen in Figure 7)[76].

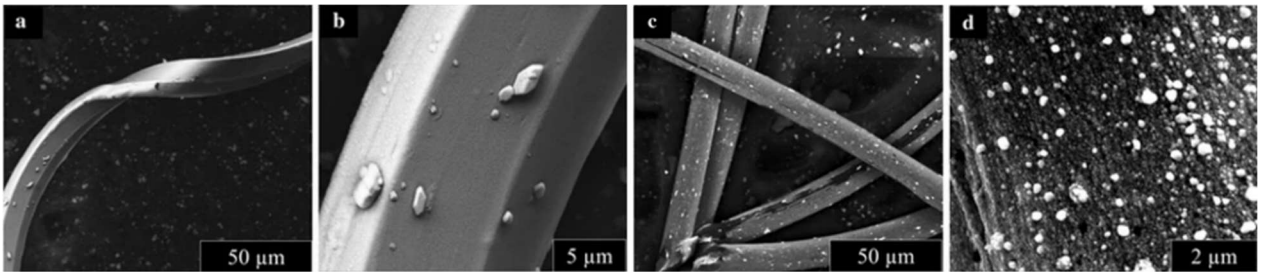

Figure 7: Two commercialized wound dressing bandages containing silver NPs. SEM images (a, b) show dressing 1, where pre-made silver NPs are directly added into the fiber material, whereas (c, d) show dressing 2 where silver NPs are grown on the fiber surface[76].

Wound dressing nanocomposites can be made of many materials, such as polyvinyl alcohol (PVA), cellulose, and polyethylene oxide (PEO)[77–79]. Depending on the nanocomposite morphology, there can be a rapid or slow release of silver NPs upon contact with moisture and

fiber wetting[76]. This release allows for continuous sterility of the bandaged area even with long application durations. In real world usage, moisture from skin would allow silver NPs to diffuse out of the wound dressing material and into or around the exposed lesion area. This keeps open wounds sterile and provides a reliable barrier to infection that can effectively kill bacteria regardless of the presence of antibiotic-resistant strains.

In a paper by Li et al., Ag NPs were produced using chitosan oligosaccharide (COS) as a reducing agent, then electrospun into PVA fibers[78]. These fibers were then formed into wound dressing bandages. A zone of inhibition test was executed to ensure that the composite had antimicrobial properties against both *S. aureus* and *E. coli*, and would ensure sterility on the applied wound area. Pre-clinical tests were also performed in-vivo on rabbits for skin irritation and inflammation, as well as mice to study wound healing time. The results of the wound healing study proved that the scars covered by the Ag NP-COS-PVA nanocomposite was able to heal much quicker compared to wounds covered in regular gauze, and there was minimal irritation to the skin[78]. These results encourage continuous development of silver NP wound dressing materials.

2.6.2 Food Packaging Nanocomposites

Food facilities must be bacteria-free to ensure the health of consumers, thus food packaging materials can benefit from antibacterial nanocomposites as well. Xu et al. prepared starch films reinforced with CNC and grape pomace extract (GPE) for food packaging applications[80]. Grape pomace refers to the solid remains following pressing for juice or winemaking, consisting of skin, pulp, stems, and seeds; they contain a high level of polyphenols which exhibit strong antimicrobial activities[80]. In their paper, CNC was used as a reinforcing filler while GPE was used as a functional bactericidal agent. The nanocomposite films had increased mechanical properties, and the CNC

facilitated more phenolic compound release from the GPE. Overall, the GPE-CNC-starch films presented effective inhibition of *S. aureus* and *L. monocytogenes.* The natural materials used for this nanocomposite make them ideal for food packaging due to their inherent non-toxicity, biodegradability, and renewability, while also ensuring safe bacteria-free foods for the consumer.

Antibacterial CNC have not frequently been used in nanocomposite materials, although the modification of CNC with bactericidal agents has been very well-studied. Most antimicrobial nanocomposites incorporate both CNC and an additional antibacterial additive in order to exhibit activity against the growth of microorganisms. There are very few that study the modification of CNC prior to incorporation within a polymer matrix. From literature, the antibacterial modification of CNC in rubber compounds specifically has not yet been studied. Elastomers such as NR and NBR could benefit from a functional reinforcing filler that imparts bactericidal activity.

2.7 Summary

This literature review has given an overview on rubber processing techniques, common additives, and emerging nanomaterials used in elastomeric composites. The novelty of nanomaterials in recent years has encouraged the investigation of nanosilica, nanoclay, graphene oxide, and carbon nanotubes in rubbers. However due to the increasing desire for ecofriendly product development, cellulose nanocrystals will be explored in detail in this research as both a reinforcing filler and a functional filler. By implementing CNC modification techniques studied in recent literature, cellulose nanocrystals will be functionalized as antimicrobial carriers for silver nanoparticles. This thesis will further progress the field to showcase CNC as an ideal sustainable strengthening filler through its ability to percolate, and then modify the CNC to contribute to the development of a

bactericidal elastomeric nanocomposite. It has been shown that antibacterial nanocomposites have a wide range of capabilities, whether for wound dressing or food packaging applications in polymeric matrices such as PU, PVA, or starch. The nanocomposites synthesized in this thesis will therefore enrich the field with the creation and analysis of advanced rubber thin films for use in industrial products such as gloves.

CHAPTER 3

Reinforcement of rubber thin sheets by percolation of pristine cellulose nanocrystals

---

3.1 Introduction

Research on the use of bio-based material rather than fossil fuel-based synthetic polymers is of considerable value due to the increasing interest in biodegradable and ecofriendly products. This chapter describes an in-depth analysis of the effect of cellulose nanocrystals (CNC), a promising nanomaterial filler derived from cellulosic biomass, on the mechanical properties of rubber latex thin sheets. Sheets of styrene butadiene rubber (SBR) and its bio-based alternative, natural rubber (NR) were tested and compared.

Styrene butadiene rubber is one of the most common synthetic rubbers, where the vast majority of SBR applications are for tires[81]. It is also used for footwear, hoses, seals, conveyor belts, and adhesives[81,82] due to its high toughness and abrasion resistance. SBR is a relatively inexpensive elastomer with many applications, but when SBR products are discarded, large amounts are destined for landfill and cannot be broken down through natural degradation. In the interests of environmental protection, a green polymer alternative should be considered, such as natural rubber. As aforementioned, NR occurs organically in nature and is obtained from the sap of *Hevea brasiliensis* trees[9]. NR is very versatile and an ideal alternative to SBR due to their similar properties. In fact, NR can be used for the most of the same products as SBR[14] as well as for single-use plastic products, such as balloons, rubber bands, tubes, and gloves. NR possesses excellent strength, elasticity, fatigue resistance, and good abrasion resistance[83,84]. The advantage of NR over SBR is that it is derived from a sustainable resource, but also its relatively enhanced biodegradability.

In this study, CNC was used to enhance SBR and NR properties. CNC has great potential to become an ecofriendly filler for the strengthening of plastics due to its excellent mechanical properties and high aspect ratio. This study examined the distribution of CNC in the rubber matrices, tensile properties, water permeability, and water absorption properties of the nanocomposite thin sheets below and above the percolation threshold. Percolation is an ideal phenomenon in rubber thin sheets, as the interconnected filler can significantly alter the nanocomposite properties beyond the critical point of network formation. A continuous filler network can also result in better durability: rigid fillers can create an intricate phase in the sheets, such that chemicals and cracks can be arrested. This is critical in most dipped rubber products, thin sheets, and films, as the resistance of the materials to tear propagation is an important property to ensure resilience throughout the product lifetime. Tear strength was also studied in this research, as it is a vital attribute of thin sheet rubber products. To the best of our knowledge, the tear strength of NR-CNC and SBR-CNC nanocomposites has not been reported in the literature. The effect of percolation of CNC on the tear strength of rubber sheets largely determines the viability of CNC as a strengthening filler.

3.2 Experimental

3.2.1 Materials

CNC derived by sulfuric acid hydrolysis was supplied by CelluForce Inc. It was provided in the form of an aqueous gel dispersion containing 8 wt.% CNC, and also as a freeze-dried powder. The CNC had an average length (L) of 200 nm, and an average diameter (d) of 5 nm. Styrene butadiene rubber and low ammonia natural rubber were purchased from Chemionics Corporation in latex

form. The solid content of the SBR and NR dispersions were 51.9 wt.% and 62.9 wt.%, respectively.

3.2.2 Nanocomposite Thin Sheet Fabrication

Thin sheets of SBR and NR were fabricated, reinforced with varying concentrations of CNC from 0.5 phr to 8 phr (parts per hundred rubber by dry weight). Neat NR and SBR sheets were also prepared. To create the sheets, solution mixing was carried out. A 2 wt.% CNC stock dispersion was first prepared by diluting the 8 wt.% gel CNC dispersion with DI water. This dispersion was homogenized (PowerGen 700, Fisher Scientific) for 2 minutes, followed by sonication (Fisherbrand Model 120 Sonic Dismembrator, Fisher Scientific) for 3 minutes at 60 kW and 100% amplitude to ensure that the CNCs were well-dispersed. A vacuum oven was used on the CNC stock dispersion to ensure any bubbles were removed from the liquid prior to latex incorporation.

For each batch of sheets, the required amount of 2 wt.% CNC was measured into a beaker. The dispersion was stirred continuously as the rubber latex was poured slowly into the mixture. High speed magnetic stirring was then employed for a total of 6 minutes to thoroughly mix the latex and CNC components.

The prepared latex-CNC mixtures were cast into Petri dishes to form thin sheets. The cast amount was kept constant at a dry weight of 4 g, in order to mitigate thickness variation in the final products. Drying was performed on a level surface at room temperature, where the solvent was evaporated until a constant weight was reached. The sheets were then peeled and subsequently tested for their mechanical properties. It was ensured that no bubbles were observed in the films, both visually and using optical microscopy, prior to testing the samples. CNC was the only filler

added to the latex to determine its effect on the rubber properties without masking by other additives.

3.2.3 Evaluation of Filler Dispersion

The dispersion of CNC in the rubber thin sheets was evaluated using Scanning Electron Microscopy (SEM). NR and SBR sheets containing 0 phr, 1 phr, and 6 phr of CNC were cut into approximately 1 cm x 1 cm squares. The samples' cross-sectional areas were analyzed under SEM to examine the morphology of the nanocomposite materials. Due to the high aspect ratio of CNC, it is expected to form an interconnected network at fairly low concentrations. This is known as filler percolation. The minimum volume fraction of CNC required to achieve percolation, known as the percolation threshold, can be calculated from the statistical percolation theory for cylindrically shaped filler [48,85,86]:

$$Percolation\ threshold = \frac{0.7}{aspect\ ratio} \quad (1)$$

CNC used in this project had an average aspect ratio (L/d) of approximately 40, thus the percolation threshold was expected at a concentration of 1.75% v/v of CNC. Using a density of 1.5 g·cm^{-3} for CNC[87], and a density of 0.92 g·cm^{-3} for both NR and SBR[14,82], this translates to 2.85 wt.% as the expected percolation threshold of CNC (or 2.93 phr). Above this value, a continuous network of CNC will be formed in the matrix. This theoretically calculated value assumes no aggregate formation in the thin sheets, and good dispersion of the CNC in the rubber matrix.

Transmission Electron Microscopy (TEM) (Philips, CM 10) was also performed on cryotome sections of NR and SBR containing 1 and 6 phr of CNC, to visually confirm nanoparticle percolation. Due to the softness of the rubber samples, small sections of the thin sheets were first

embedded in epoxy resin prior to cryomicrotoming at -60 °C. Small cryosections were then placed on a copper grid and subsequently imaged on the TEM.

3.2.4 Tensile Testing

A Bruker Universal Testing Machine was used for tensile testing, with a load cell of 10 kg. Sample conditioning was conducted at room temperature in accordance with ASTM D882-18 (Standard Test Method for Tensile Properties of Thin Plastic Sheeting). Minor modifications to the standard testing parameters were performed, where a strain rate of 30 mm/min and sample dimensions of 1 cm x 3 cm were used. The Yield strength and Young's modulus values were recorded, and the average values from three specimens of each formulation were reported.

3.2.5 Tear Strength Testing

The tear strength properties of each formulation were tested in accordance with ASTM D624 - 12, with some modifications to the specimen dimensions. Type T trouser tear test pieces were prepared with a size of 5 cm x 2 cm, and a tear initiation of 2 cm. Five samples from each batch were tested in a Bruker Universal Testing Machine with a load cell of 10 kg, and a strain rate of 50 mm/min.

3.2.6 Permeability Testing

Moisture barrier properties of the thin sheets were tested to determine the effect of CNC on the permeability of latex. The test conditions complied with ASTM E96 for the water vapor transmission of materials. Glass cups with a mouth area of 10.1 cm^2 were used, and sheets with a thickness of 0.75 ± 0.05 mm were secured tightly to the cups, then weighed every 24 hours. Water vapour transmission (WVT) was calculated as follows[88]:

$$WVT = \frac{G}{t \cdot A} \quad (2)$$

where G is the weight change in grams, t is time in hours, and A is the test area of the cup mouth in m^2.

3.2.7 Water Absorption Testing

A modified protocol for ASTM D570 - 98 was used for water absorption testing. Samples were cut into 25.4 mm x 25.4 mm (1 in x 1 in) squares, with a thickness of approximately 0.75 mm. The specimens were conditioned by oven drying at 50 °C for 24 hours, followed by cooling in a desiccator for 12 hours. Upon their removal from the desiccator, samples were weighed to the nearest 0.0001 g and immersed in DI water at 23 °C. Three replicate tests were performed for each sample, and the average water absorption values were calculated from the measurements.

Diffusion coefficients D for the sheets of thickness l were calculated using models proposed by Crank[89]:

$$\frac{M_t}{M_\infty} = \frac{4}{l}\left(D \cdot \frac{t}{\pi}\right)^{1/2} \quad (3)$$

where M_t is the fluid quantity that has diffused in a time t, and M_∞ is the equilibrium moisture content[89–91].

3.3 Results and Discussion

3.3.1 Filler Dispersion

NR and SBR latex were combined with pristine CNC, and no chemical modification to the CNC was performed. The thin sheet preparation method exploited the mutual dispersibility of CNC and latex in water. Since both materials could be readily dispersed in aqueous media, this allowed for facile mixing and even distribution of the filler into the rubber.

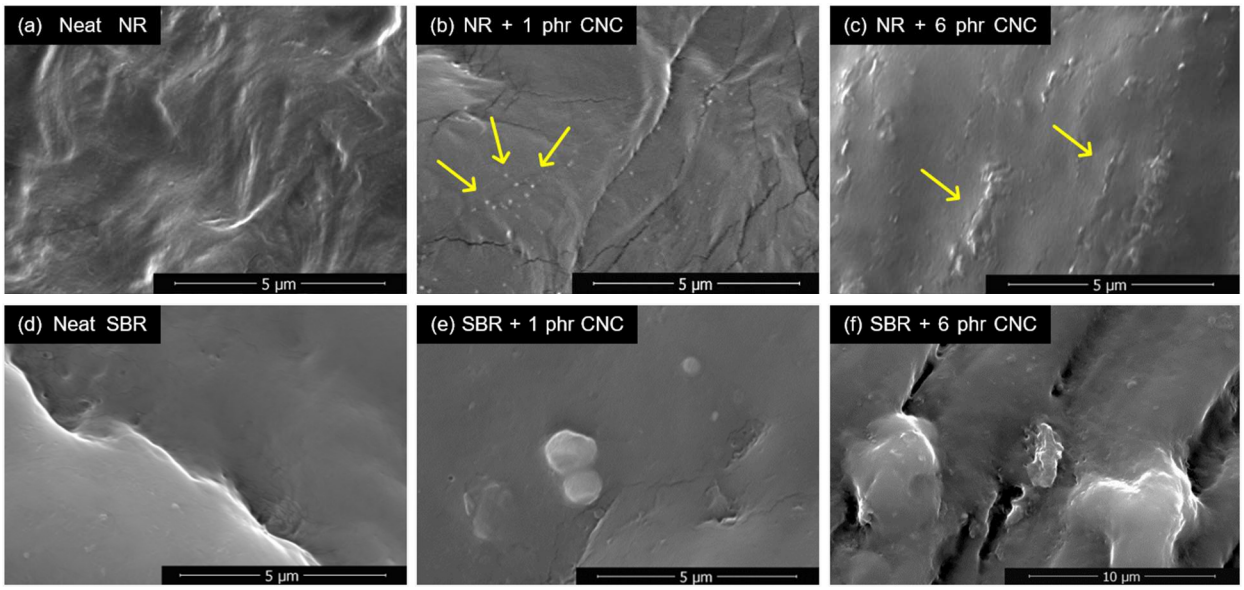

Figure 8: SEM cross-sectional images of nanocomposite sheets. CNC is well-dispersed in NR (b), and percolation is shown in the 6 phr CNC sheet (c). Agglomerates occurred in the SBR samples, depicted in (e) and (f).

SEM analysis of the sheets confirmed that CNC was well-dispersed throughout the NR. As shown in Figure 8b, arrows reveal small dots of CNC spread throughout the rubber sheet. Some percolation of the CNC was visible in the cross-section of the NR sample with 6 phr of CNC, as shown by the CNC networks (marked by the yellow arrows).

In SBR, the distribution of CNC was not as uniform as it was in NR. Aggregates occurred at both 1 phr and 6 phr of CNC with no observable percolation on SEM. Large clusters of CNC were evident instead, as shown in Figure 8e and 8f. This phenomenon is consistent with nanocomposite theory, where aggregation is a common problem with nano-sized materials[92–95] due to their high surface energy. Such poor dispersion is more pronounced when the polarity difference between the polymer matrices and the filler is high, as in the case of hydrophobic rubber (NR and SBR) and hydrophilic CNCs. A plausible explanation for the contrasting CNC dispersion within the NR and SBR nanocomposites was due to the difference in the chain structure between NR and SBR. NR consists of a chain of cis-1,4-polyisoprene, giving a linear polymer structure. Contrarily, SBR contains a styrene moiety on its polymer backbone, resulting in more steric hindrance that limits an intimate interfacial interaction with the polar CNCs. This steric hindrance could promote the migration of the hydrophilic CNC toward areas of water in the SBR thin sheets as the sheets dried during the casting process.

TEM images were better able to demonstrate CNC percolation within the samples. As seen in Figure 9, NR and SBR samples with low loading (1 phr CNC) could form very short networks with one another. Similar to the SEM, the TEM images indicated that the dispersion of CNC was less uniform in SBR, as the CNC agglomerated in small areas rather than dispersed evenly throughout the thin sheet. For high loading (6 phr of CNC) in NR, the presence of fully percolated networks was evident as per Figure 9b. Percolated networks were observed in SBR at high CNC loading, but the structure showed very fine webs. It is likely that this is due to aggregation of CNC in other areas of the thin sheet, thus there were much less CNC available for continuous filler network formation.

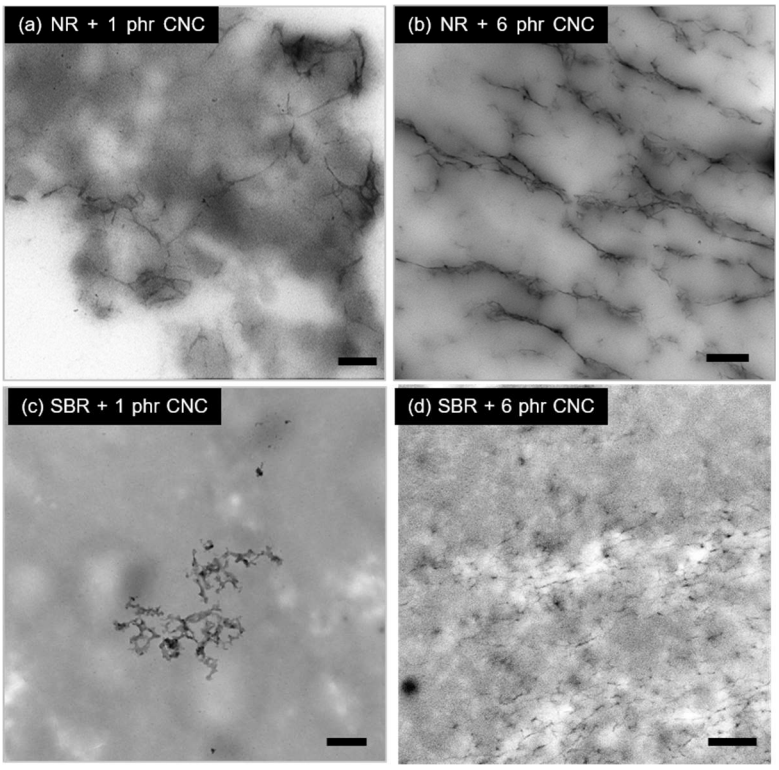

Figure 9: TEM images showing CNC percolation in the thin sheets of rubber. Scale bars represent 1 μm.

3.3.2 Mechanical Properties

Generally, nanofillers can achieve high levels of rigidity at much lower loading levels than conventional fillers[94] because of their high specific surface area. The mechanical properties of the CNC-filled NR and SBR nanocomposites were evaluated to determine the effect of CNC on the mechanical properties. Representative tensile curves for each formulation, as well as the yield strength and modulus for the NR-CNC and SBR-CNC nanocomposites are shown in Figure 10.

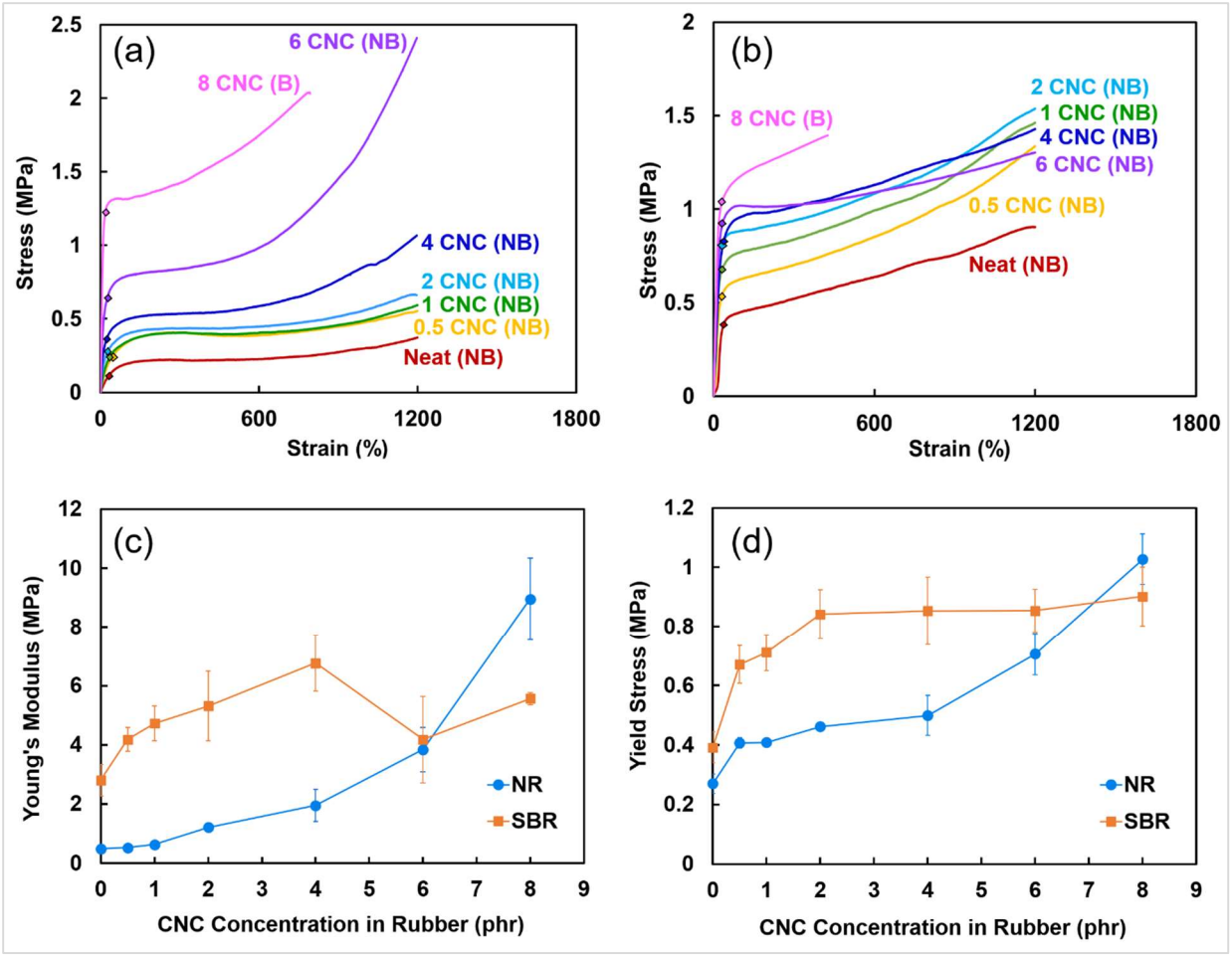

Figure 10: Representative tensile curves for (a) nanocomposite NR sheets and (b) nanocomposite SBR sheets, with varying CNC concentration in phr. "B" denotes the full break of a sample due to high filler loading and limited chain mobility, whereas "NB" denotes non-break for samples that stretched to the limits of the tensile machine. Point markers indicate the yield point of each sample. Trends in (c) Young's modulus and (d) yield stress of NR and SBR nanocomposite sheets with CNC filler are also shown.

For NR, there is an evident positive correlation between both Young's modulus and the yield strength with increasing CNC loading in the thin sheets. Stress is transferred from the elastomeric matrix to the rigid CNC nanofiller material when force is applied[96], resulting in a higher modulus. Thus, CNC acted as a reinforcing filler within the thin sheets. CNC is also shown to increase the yield strength of the NR nanocomposite, whereas micro-sized fillers typically

reduced the yield strength at higher loading[97]. In the concentration range being examined, both the yield strength and modulus of the NR increased with increasing volume fraction of CNC fillers due to the small particle size[97].

In the SBR sheets, the reinforcing effect of CNC was not as prominent as that of the NR nanocomposite sheets. The Young's modulus of samples increased until 4 phr, and above this filler concentration, there was a drop in the modulus value that could be attributed to the aggregation of CNC. Due to the reduced interaction between the filler and the rubber matrix, the CNC was not able to transfer as much stress between the polymer chains. Instead, the agglomerates acted as weak points in the matrix that facilitated crack propagation. The yield strength of the SBR nanocomposite displayed a dramatic increase at 1 and 2 phr CNC loading. The increase was 81% and 115% for the 1 and 2 phr CNC reinforced nanocomposites, respectively, indicating an effective load transfer from the SBR to the CNC at these loading levels. Beyond the 2 phr loading levels, the CNC did not provide a statistically significant strength improvement. Again, this could be attributed to the aggregation of CNC at high loading, resulting in negligible change in the yield strength values between 2, 4, 6, and 8 phr of CNC. Larger aggregates at higher loading tend to mimic the effect of micro-sized particles on the properties[93], as the nanoparticle clusters have an effective diameter in the micron range.

The effect of CNC fillers on the cut growth of the rubber nanocomposites under tension was evaluated using the trouser cut (Die T) method in accordance with ASTM D624 -12. At higher CNC loading ranges, the tear strength properties of the NR and SBR nanocomposite samples displayed a positive correlation with the CNC content. At low concentrations, however, CNC did not have a significant strengthening effect during tearing. Figure 11 shows the tear strength of

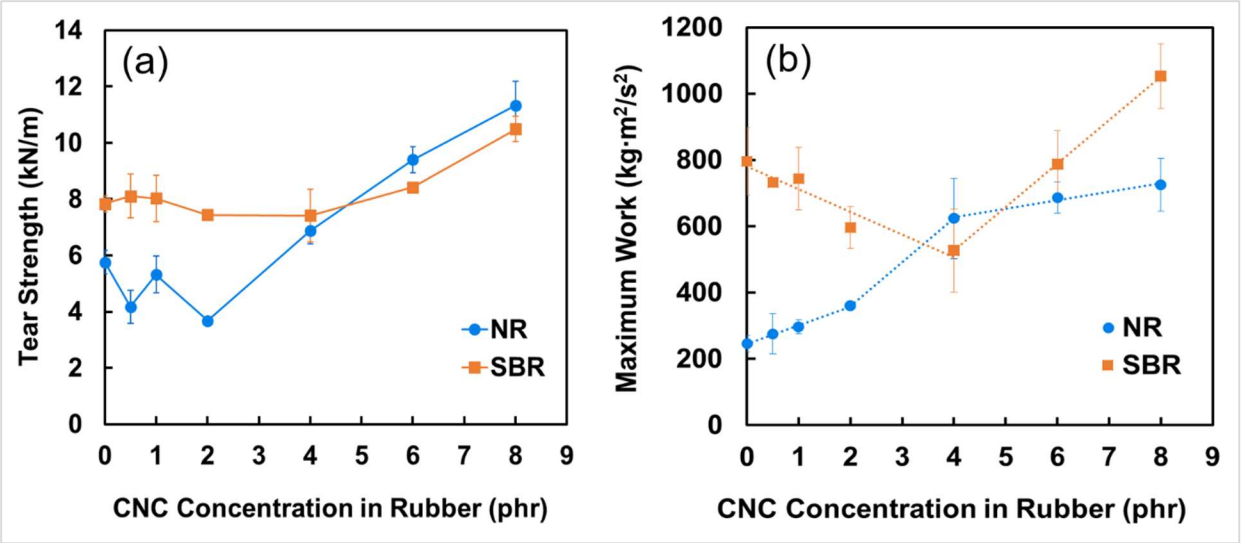

Figure 11: Tear test results of nanocomposite NR and SBR sheets containing increasing CNC content. Tear strength (a) and maximum work required to tear (b) are shown.

samples against the CNC concentration in the sheets, as well as the maximum work required to completely tear the rubber samples.

Based on the graphs, there was a clear jump in both the tear strength and maximum work required to fully tear a NR sample from 2 phr to 4 phr of CNC. An increase in tear strength and maximum work also occurred in the SBR sheets above 4 phr of CNC. This result further confirmed the presence of percolation of CNC in the sheets. As discussed earlier, the percolation threshold of CNC is expected at a concentration of 2.93 phr, which supported the experimental results of the NR-CNC nanocomposite, where CNC concentrations at 4 phr and above demonstrate high resistance to tearing.

Meanwhile, the percolation threshold of CNC in SBR was experimentally higher than the anticipated value. Reinforcement due to percolation occurred between 4 phr and 6 phr, likely due to the relatively poor interfacial interaction between the SBR and CNC that led to aggregation of

CNC in the sheets. Since the filler was not well-dispersed, a concentration higher than 2.93 phr of CNC was required to form a percolated network. Despite the aggregation of the filler, some CNC were still able to form a network as shown by the increase in tear strength at high loadings (6 and 8 phr).

Figure 12 depicts the proposed mechanism of filler reinforcement on the tear strength of thin sheets. When the filler concentration is low, the rubber is easily torn along the path of least resistance: that is, through areas where there is no CNC in the rubber. Closer to the percolation threshold, CNC began to form larger interconnected structures, but there were still regions that were not reinforced. At these concentrations, the tear can propagate along the interface between CNC and the polymer chains if there is weak interfacial adhesion between the two, as is the case with SBR. Because there are only weak van der Waals interactions between the CNC and rubber matrix, the tearing occurred most readily at the CNC-rubber interfacial boundary and required less force to break because of weak filler-matrix interactions. The polymer was locally stretched at these zones around the rigid CNC, creating voids until complete rupture[98]. Above the percolation threshold, the network of linked CNC must be broken in order to tear the samples. This requires

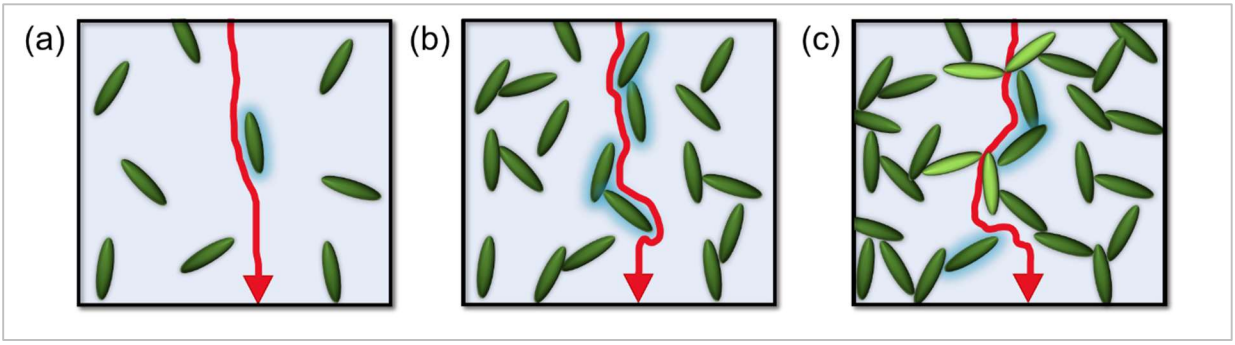

Figure 12: Effect of percolation on the tear strength of sheets with (a) low filler content, tear goes along path of least resistance (b) close to percolation threshold, crack propagation due to weak filler-matrix interactions, and (c) percolated network, strong filler-filler interparticle forces must be broken to tear the sample.

higher energy; hence the jump in tear strength once percolation occurred. Due to the agglomeration of CNC in the SBR sheets, the trend in Figure 11 initially showed a decreasing maximum work (from 0 until 4 phr of CNC filler), which could be attributed to the larger effective surface area between the CNC and SBR allowing for easy tearing at the large weak interface. This decrease was not evident in the NR sheets, since the CNC filler was well-dispersed. Overall, the results indicate that the high aspect ratio CNCs were beneficial to reinforce the thin sheets against tearing via percolation.

To confirm the proposed mechanism in Figure 12, SEM imaging was performed on the fracture surfaces of tear test specimens. In Figure 13a and 13d, both neat NR and SBR samples display brittle fracture surfaces with no apparent deformation prior to failure. In comparison, some

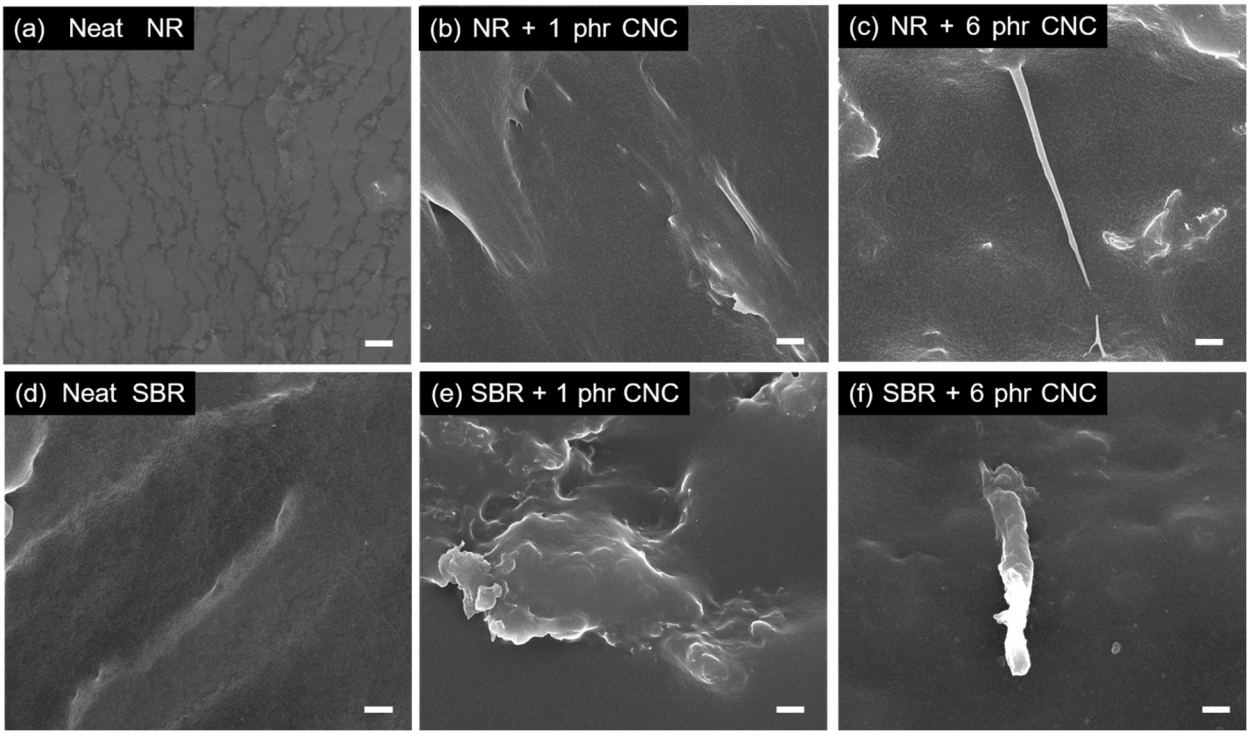

Figure 13: SEM images of the fracture surfaces of tear strength samples. Fibrillation is visible in (b) NR + 1 phr CNC; (c) NR + 6 phr CNC; and (f) SBR + 6 phr CNC. Scale bars represent 1 μm.

fibrillation is visible in the NR sample containing 1 phr of CNC as the networks of CNC start to strengthen the sheet and create tortuosity along the path of failure. The samples containing high loading of filler (NR and SBR with 6 phr of CNC) display very evident fibrillation and therefore indicate ductile fracture modes in these thin sheets[99]. These high loading nanocomposites show that the percolated network of CNC caused a slower failure mode and therefore more extensive deformation of the rubbers. Due to the high energy required to break apart the CNC bonds, they caused long fibrils to form during fracture since they are embedded in complex networks throughout the polymer material. Meanwhile, very little to no fibrillation is visible in Figure 13e which shows the SBR nanocomposite containing 1 phr of CNC. As previously discussed, this sample contains aggregates and therefore it is likely to follow the mechanism suggested in Figure 12b, easily allowing tear propagation along the interface of the filler and polymer chains.

3.3.3 Water Permeability & Absorption Properties

Due to the hydrophilic nature of CNC, its presence in the rubber thin sheets increased the water permeability properties. This is shown in Figure 14, which depicts the water vapour transmission (WVT) rate through the nanocomposites. Typically, NR and SBR are excellent water barriers. The results indicated that upon the incorporation of CNC to NR and SBR, a more permeable nanocomposite rubber was produced. This nanocomposite would be useful for applications that require some moisture passage allowing water vapour to pass more easily through the sheets. For instance, separation membranes or gloves that require moisture removal during use could benefit from the higher water vapor transmission rate of the CNC filled rubber nanocomposites.

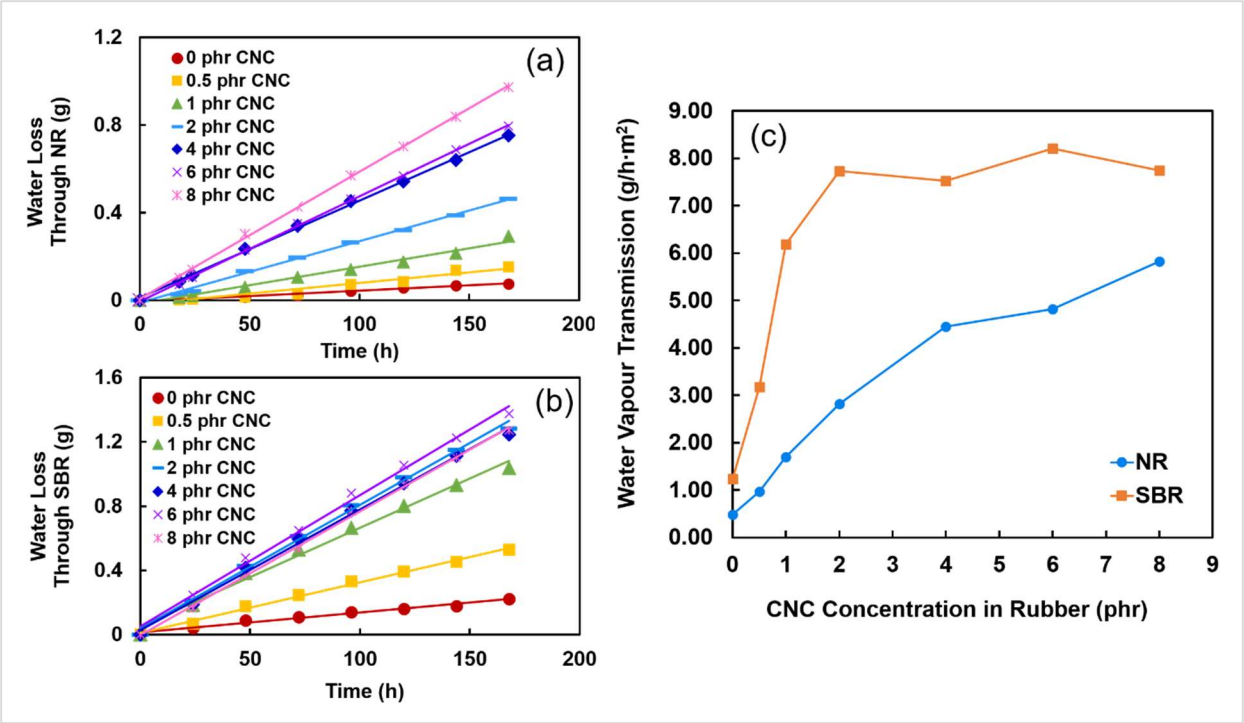

Figure 14: Water vapour transmission through nanocomposite sheets of (a) NR-CNC and (b) SBR-CNC, where (c) shows the trends in water vapour transmission rate as the filler concentration increases.

The water absorption properties of the sheets were also examined. Rubbery polymers generally exhibit Fickian diffusion[89], and models were fitted to the absorption values using correlations described in Eq. (3). Based on the initial linear weight change of nanocomposite sheets over the immersed time ($M_t/t^{\frac{1}{2}}$), as well as the maximum absorption of the sheets (M_∞), diffusion coefficients through the reinforced polymers were calculated from the data in Figure 15b and 15c, and results are presented in Figure 15a. Although CNC is extremely hydrophilic, we observed that the overall diffusion coefficient values were still quite low in both systems. The highest diffusion coefficients were in the range of tenths of a square millimeter per hour. Hence, we concluded that CNC did not significantly impair the water resistance of the polymer sheets despite increasing the rate of diffusion for both NR and SBR.

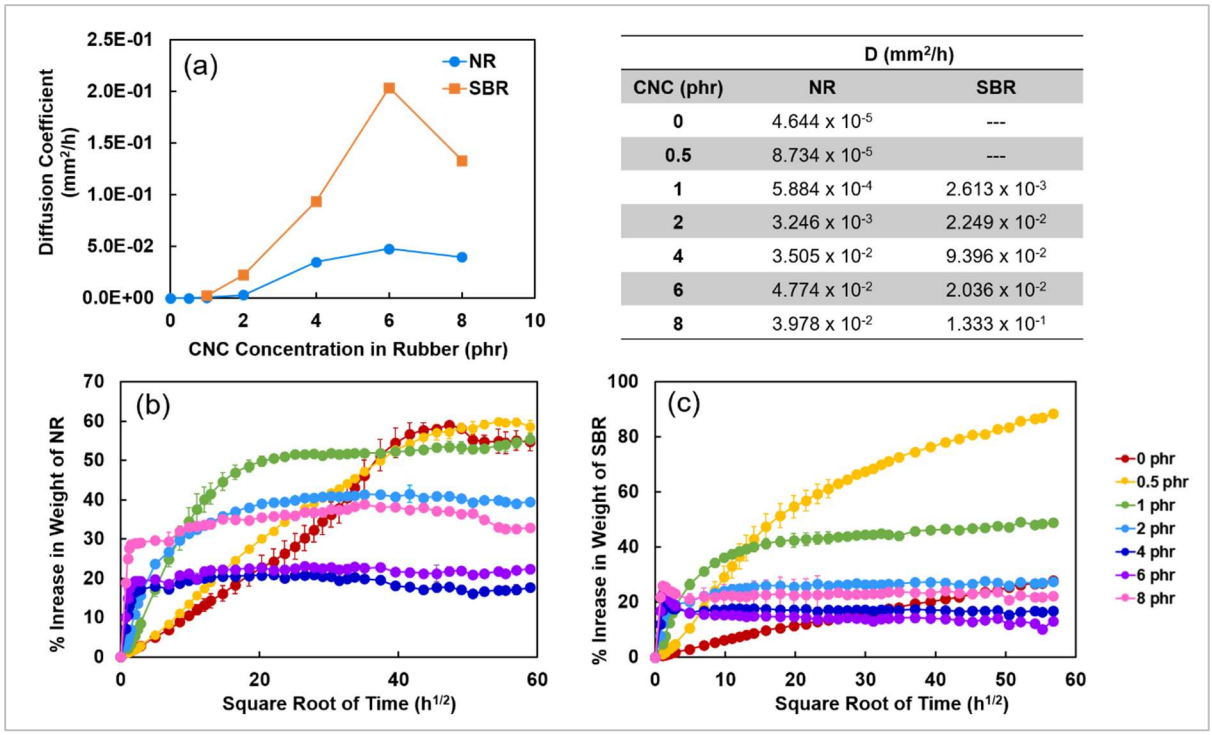

	D (mm²/h)	
CNC (phr)	NR	SBR
0	4.644×10^{-5}	---
0.5	8.734×10^{-5}	---
1	5.884×10^{-4}	2.613×10^{-3}
2	3.246×10^{-3}	2.249×10^{-2}
4	3.505×10^{-2}	9.396×10^{-2}
6	4.774×10^{-2}	2.036×10^{-2}
8	3.978×10^{-2}	1.333×10^{-1}

Figure 15: Diffusion coefficients of water through NR-CNC and SBR-CNC sheets(a), calculated from the water absorbance graphs of NR (b) and SBR (c).

The coefficient values reinforced the percolation phenomenon observed in the SEM and tear results. In NR, diffusion was extremely slow for neat NR as well as sheets with 0.5 and 1 phr CNC content, since the filler particles across the matrix were far apart. The CNC could facilitate the absorption of some water molecules through hydrogen bonding, but water uptake into the sheets was extremely slow due to the non-polar NR polymer chains. At 2 phr, the CNC were very close to their percolation threshold resulting in the formation of long fibrous networks. Although these CNC networks may not have spanned across the entire sheet, they resulted in a higher water uptake compared to the low concentration nanocomposites. Finally, once the percolated CNC network was formed (4, 6, and 8 phr CNC in NR) the diffusion coefficient increased by nearly a factor of 1000 %. The percolated CNC allowed for a continuous path along which water molecules

could easily travel through the rubber sheets. The highly hydrophilic CNCs were able to form hydrogen bonds with numerous neighbouring water molecules, readily transferring them along the CNC surface and into the NR matrix. The jump in diffusion coefficient is visually depicted in Figure 15a.

SBR nanocomposite sheets showed similar trends, where the large jump in diffusion coefficient was again observed in Figure 15. Two large increases occurred between 2 and 4 phr, as well as between 4 and 6 phr CNC due to the filler agglomeration in the sheets. The large clumps of CNC resulted in much higher concentrations required to form percolated networks in the SBR matrix, but they were able to uptake much more water compared to the CNC that was well-dispersed in NR. Since the CNC in SBR were in close contact and formed many aggregates, the aggregates were able to absorb large amounts of water into the SBR rubber sheet.

Diffusion coefficients were not calculated for the neat SBR and 0.5 phr CNC in SBR sheets, as the sheets were not able to reach a steady state absorption value within the allocated test time. It is hypothesized that the large side chains present on the SBR structure hinders water absorption, as SBR has a branched structure containing phenyl groups. As such, diffusion was extremely slow when investigated here, and it will be a subject of future study.

3.4. Conclusions

The results of this study show that the incorporation of CNC in both natural and synthetic rubber latexes led to enhanced mechanical properties. The bio-based filler had a positive effect as a reinforcing filler on the modulus and yield strength of NR and SBR sheets. Of particular importance was the significant improvement in the tear strength of the nanocomposite thin sheets,

which was observed to increase largely due to the percolation of the filler within the polymer matrices. The CNC improvement on tear strength could allow for the production of extremely thin rubber sheets with high durability and toughness. Overall, since CNC was able to enhance the material properties yielding stronger rubber sheets, it can be considered an excellent candidate as a sustainable and ecofriendly option compared to some other reinforcing fillers. Its high aspect ratio is unique for achieving percolation, and thus superior resistance to crack propagation in the matrix. Due to its nanosize and renewability, CNC is a very promising filler to strengthen rubber films or thin sheets and potentially other highly cured products.

CHAPTER 4

Antimicrobial rubber nanocomposites using modified cellulose nanocrystals and silver nanoparticles

4.1 Introduction

The overuse of antibiotics and the rise of antibiotic resistance pose serious problems as bacteria evolve to withstand treatment by traditional methods. In fact, antibiotic resistance has been identified by the World Health Organization as one of the biggest threats to global health, food security, and development today[100]. Due to the newfound resilience of bacterial strains, common infections are at risk of becoming much more dangerous threats to human health, requiring time-consuming or costly treatment[55,101].

In the medical field, surgical site infections are a common issue that patients must combat as they heal from open wounds. Up to 77% of surgical patient deaths are reported to be infection-related[102] rather than caused by complications in the surgery itself. The need for better prevention of cross-contamination and higher sterility must therefore be addressed in order to reduce the chances of infection.

In this chapter, the development of a novel antimicrobial rubber material is explored. This thin film material could be useful in the production of medical gloves, which would mitigate the risk of infections by killing bacteria and preventing the spread of harmful microorganisms. Due to the large amounts of waste generated by hospitals[103,104], this project also focuses on the use of sustainable chemistry and engineering in the material synthesis and product formulation.

Silver nanoparticles (Ag NPs) were used as the active antimicrobial agent. Silver is well-known to possess antibacterial properties[56], and it is considered more versatile than antibiotics at killing bacteria due to the various ways in which they can attack the cell, causing bacterial lysis and preventing replication[68,72,73]. However, as Ag NPs have a high surface energy, they are prone

to aggregation in solution. The NPs will therefore be stabilized on cellulose nanocrystals (CNC), which are hydrophilic and have the added advantage of acting as a reinforcing filler within the rubber matrix, due to the large aspect ratio of CNC rods.

To the best of our knowledge, antimicrobial-modified CNC has not previously been studied in rubber latex formulations. This work explores the potential of modified CNC as a dual-purpose filler, imparting both strength and bactericidal capabilities to the rubber. The production of rubber composites using such materials may have applications in medical or food handling sectors, and the modified CNC filler can be further extended for use in other materials to prepare antibacterial coatings or textiles for advanced applications where sterility is essential.

4.2 Experimental

4.2.1 Materials

Silver nitrate ($AgNO_3$), calcium nitrate ($Ca(NO_3)_2$), 4-(2-hydroxyethyl)-1-piperazineethanesulfonic acid (HEPES buffer), sodium hydroxide (NaOH), tannic acid (TA), polyethylene glycol tert-octylphenyl ether (Triton surfactant), and zinc oxide (ZnO) were purchased from Sigma-Aldrich. Sulfur (S) was purchased from Acros Organics. Calcium carbonate ($CaCO_3$) and zinc dibutyldithiocarbamate (ZDBC) were purchased from Fisher Scientific. CNCs were supplied by CelluForce Inc. in powdered form. The average length and diameter of the CNC was 200 nm and 5 nm, respectively.

To prepare rubber films, low ammonia natural rubber (NR) and nitrile butadiene rubber (NBR) latex were purchased from Chemionics Corporation. The solid content of the NR dispersion was 62.9 wt%, and the NBR dispersion contained 47.1 wt% solids.

Antimicrobial tests were performed with plate count agar, nutrient broth, and phosphate buffered saline (PBS) powder from Fisher Scientific and bacteria from Cedarlane Laboratories.

4.2.2 Preparation of CNC-TA-Ag

CNC-TA-Ag antimicrobial nanoparticles were prepared by modifying CNCs in aqueous solution. The optimization of the synthesis method was performed by testing various pHs and molar ratios of TA:Ag to achieve the best Ag deposition on CNC (see Supplementary Information - Section 4.5). The final procedure is outlined below, where the process is split into two parts: first, depositing TA onto the CNC surface and second, depositing Ag onto the CNC-TA.

In the first part of the process, TA was deposited onto the CNC surface using a green process adapted from Hu et al.[105]. First, a 1 wt% CNC dispersion was prepared by homogenizing 4.0 g CNC powder in 400 mL DI water for 10 minutes. A bath sonicator was then used on the solution for 20 minutes to ensure that the CNCs were well-dispersed. HEPES buffer (0.96 g) was added directly to the CNC dispersion, and the pH was adjusted to 8.0 using NaOH. In a separate beaker, 400 mg of TA was added to 16 mL of deionized water and mixed for 1 minute. This TA dispersion was combined with the CNC dispersion, and the mixture was stirred at 200 rpm for 18 hours at room temperature to form CNC-TA.

In the second part of the process, 2.5 mg/mL solution of $AgNO_3$ was prepared for the one-pot synthesis on CNC-TA. A molar ratio of 1:20 (TA:Ag) was chosen based off initial tests (see Figure S2), due to the ability of one TA molecule to donate 20 electrons for the reduction of silver ions[64]. The appropriate amount of $AgNO_3$ solution was thus calculated and added dropwise to the CNC-TA dispersion at pH 8.0. A colour change to dark brown visually indicated the successful

synthesis of silver nanoparticles. The entire mixture was then dialyzed against DI water for four days and against miliQ water for one day, and the final CNC-TA-Ag dispersion was concentrated to 2.4 wt% solid content via rotary evaporation.

4.2.3 Transmission Electron Microscopy (TEM)

A Philips CM10 TEM was used for microscopic imaging of the CNC-TA-Ag. The aqueous suspension was diluted to 0.1 μg/mL, then drop-casted onto a carbon-coated copper grid for analysis. The grid was allowed to dry for at least 12 hours prior to TEM imaging.

4.2.4 UV-Vis Spectroscopy (UV-Vis)

A Cary 100 Bio UV-Vis spectrophotometer (Agilent Technologies) was used to characterize the CNC-TA-Ag product. The aqueous suspension of CNC-TA-Ag was diluted to a concentration of 0.1 mg/mL, and samples were run against a background of deionized water.

4.2.5 Zeta Potential Measurement

Zeta potential was determined using a folded capillary cell in a Malvern ZS90 Zetasizer. The modified CNC was diluted a concentration of 0.1 mg/mL in order to accurately assess the stability of suspension.

4.2.6 Thermogravimetric Analysis (TGA)

Thermogravimetric analysis was performed on CNC-TA-Ag with a TA Instruments Q500 TGA in order to quantify the amount of silver on the CNC. Approximately 5 mg of sample was placed on aluminum sample pans and run up to 750 °C under nitrogen atmosphere. At 110 °C, a 2 minute isothermal step was performed in order to remove any moisture trapped in the sample for a better defined degradation step.

4.2.7 Nanocomposite Film Preparation

NR and NBR films containing 0, 0.5, 1, and 3 phr of CNC-TA-Ag filler were prepared using the coagulant dipping method. The coagulant formulation and rubber formulations are shown below in Table 2, Table 3, and

Table 4, optimized to produce smooth thin films and given in terms of parts per hundred (PHR) based on latex solid content.

Table 2: Coagulant formulation for dipping method

Component	Purpose	PHR
Water	Solvent	100
Calcium nitrate	Coagulant	0, 0.5, 1.5, 3
Calcium carbonate	Helps former release	0.05
Triton	Surfactant	1.1

Table 3: Natural rubber latex formulation for dipping method

Component	Purpose	PHR
NR	Rubber matrix	100
CNC-TA-Ag	Filler	0, 0.5, 1.5, 3
3% KOH solution	pH modifier	0.05
S	Crosslinker	1.1
ZDBC	Accelerator	0.7
ZnO	Activator	1.3

Table 4: Nitrile butadiene rubber latex formulation for dipping method

Component	Purpose	PHR
NBR	Rubber matrix	100
CNC-TA-Ag	Filler	0, 0.5, 1.5, 3
3% KOH solution	pH modifier	1.5
S	Crosslinker	1.5
ZDBC	Accelerator	0.35
ZnO	Activator	0.65

The latex mixtures were prepared by combining all the ingredients together in a beaker under medium stirring. The viscosities of the mixtures were measured with a Brookfield DV-E viscometer. Due to the thickening effect of CNC on the rubber latex, the formulations were diluted with DI water to achieve the same consistency to ensure identical stirring among batches. All NR formulations were diluted to a viscosity of 34.4 cP, while all NBR formulations were adjusted to a viscosity of 49.8 cP. Pre-curing was then performed on the mixtures for 3 days under gentle stirring at room temperature.

Rectangular glass formers were used to prepare films to mimic industrial dipping processes. Warm formers were first immersed into coagulant for 10 seconds, then heated for 10 minutes in an oven at 90 °C to dry the coagulant layer onto the surface. The coated formers were then cooled to 50 °C and dipped into the rubber latex mixtures with a 40 second dwell time. Finally, the formers were dried for 45 minutes in an oven at 90 °C to set the film shape, and the solid films were gently peeled from the former surface. An additional 2 hours of post-curing was performed at 90 °C to ensure complete cross-linking in the rubber films.

4.2.8 Antimicrobial Testing

The bactericidal efficacies of the CNC-TA-Ag and rubber nanocomposite films were evaluated using minimum inhibitory concentration (MIC) tests against both Gram-negative (*Escherichia coli*) and Gram-positive (*Staphylococcus aureus*) bacteria. Two independent tests were performed, with two replicates in each. The detailed procedure adapted from Shi et al.[54] is described below.

Agar and broth preparation. Agar powder (23.5 g) was dissolved in 1000 mL of DI water in a large container until a homogeneous solution was obtained. Nutrient broth (1.15 g powder) was prepared using DI water (50 mL) in a small flask. Both solutions were then loosely covered and sterilized in an autoclave for 45 minutes. Agar plates were prepared by pouring hot agar into sterile Petri dishes in a sterile environment. The solidified plates were stored at 4 °C prior to use.

Bacterial inoculation. Nutrient broth was cooled to ~35 °C after autoclaving. One pristine bacteria colony was then transferred into the solution using a sterile wire loop, and cultured at 37 °C for 14 hours. The bacterial solution was then diluted with sterile broth until the optical density was approximately 0.07 at 600 nm.

Incubation with antibacterial materials. The CNC-TA-Ag dispersion was diluted to concentrations of 0, 2, 4, 8, 16, 32, 64, and 100 μg/mL. The rubber films were cut into 7 mm x 7 mm squares, then sterilized with 70% ethanol. In a sterile 2 mL centrifuge tube, the antibacterial material (500 μL of diluted CNC-TA-Ag solution or square rubber films) was combined with 500 μL of bacterial solution. Control samples were prepared using the same protocol, using sterile DI water in lieu of any antimicrobial material. The sample tubes were then incubated in a rotary shaker at 37 °C and 90 rpm for 20 hours.

Antibacterial evaluation. After the samples were fully incubated, 100 µL of the final solutions were plated onto agar dishes in replicates of two. Ten-fold serial dilutions were performed up to 100,000X to ensure a countable number of bacteria were present on the plates. The agar plates were placed upside down in an incubator for 18 hours to promote the colony growth. The number of colonies were then counted and compared to the control in order to determine the CNC-TA-Ag concentration that inhibited visible growth of any microbes (known as MIC).

4.2.9 Mechanical Testing

Tensile tests. The tensile properties of the NR and NBR films were evaluated using a Shimadzu AGS-X Testing Machine with 10 kN load cell. Tests were performed in accordance with ASTM D882, with a grip separation speed of 500 mm/min. Five specimens with dimensions of 7 cm x 1 cm were tested for each formulation, cut parallel and normal to the dip direction of the films to evaluate isotropy.

Tear tests. The Shimadzu AGS-X Testing Machine was used to conduct tear tests to determine the resilience of the films against tearing. Tests were conducted in accordance with ASTM D624 with some modifications to the sample dimensions. Type T trouser test samples were prepared with a size of 5 cm x 2 cm, and a tear initiation of 2 cm. Three specimens from each batch were tested with a strain rate of 50 mm/min.

4.3 Results and Discussion

4.3.1 Preparation of CNC-TA-Ag

The growing interest in green chemistry has seen an increase in the use of plant extracts for chemical reduction of metal nanoparticles[106–108]. Tannic acid, a plant polyphenol, was used in this study due to its environmentally friendly origins and non-toxicity. TA is an ideal "glue" for attaching Ag NPs onto CNC, as it is known to hydrolyze into glucose and gallic acid units under mild acidic or basic conditions[109]. Gallic acid induces the reduction of silver nitrate into Ag NPs in basic conditions, while glucose acts as a stabilizer at alkaline pH[109,110]. This makes TA effective as both a reducing and capping agent for Ag NP synthesis at pH 8. The abundance of phenolic groups in its structure allow for the formation of quinones, which subsequently donate electrons for metal salt reduction[109,111] as shown in Figure 16.

The structure of TA also allows for facile interaction between the abundant hydroxyl groups in CNC and TA (Figure 16). At alkaline pH, it is hypothesized that TA experiences a solubility reduction and intermolecular attraction forces encourage surface deposition onto CNC via hydrogen bonding[105,112], although the exact mechanism of coating is not fully understood.

4.3.2 Characterization of CNC-TA-Ag

In situ growth of silver NPs was successfully achieved on the surface of CNC-TA, as evident from the TEM analysis (Figure 17d-f). The morphology of the silver NPs is spherical, with an average diameter of 15 ± 5 nm. The TEM also revealed the final CNC-TA-Ag product possessed varying degrees of silver NP coverage, where some CNC rods were observed to have

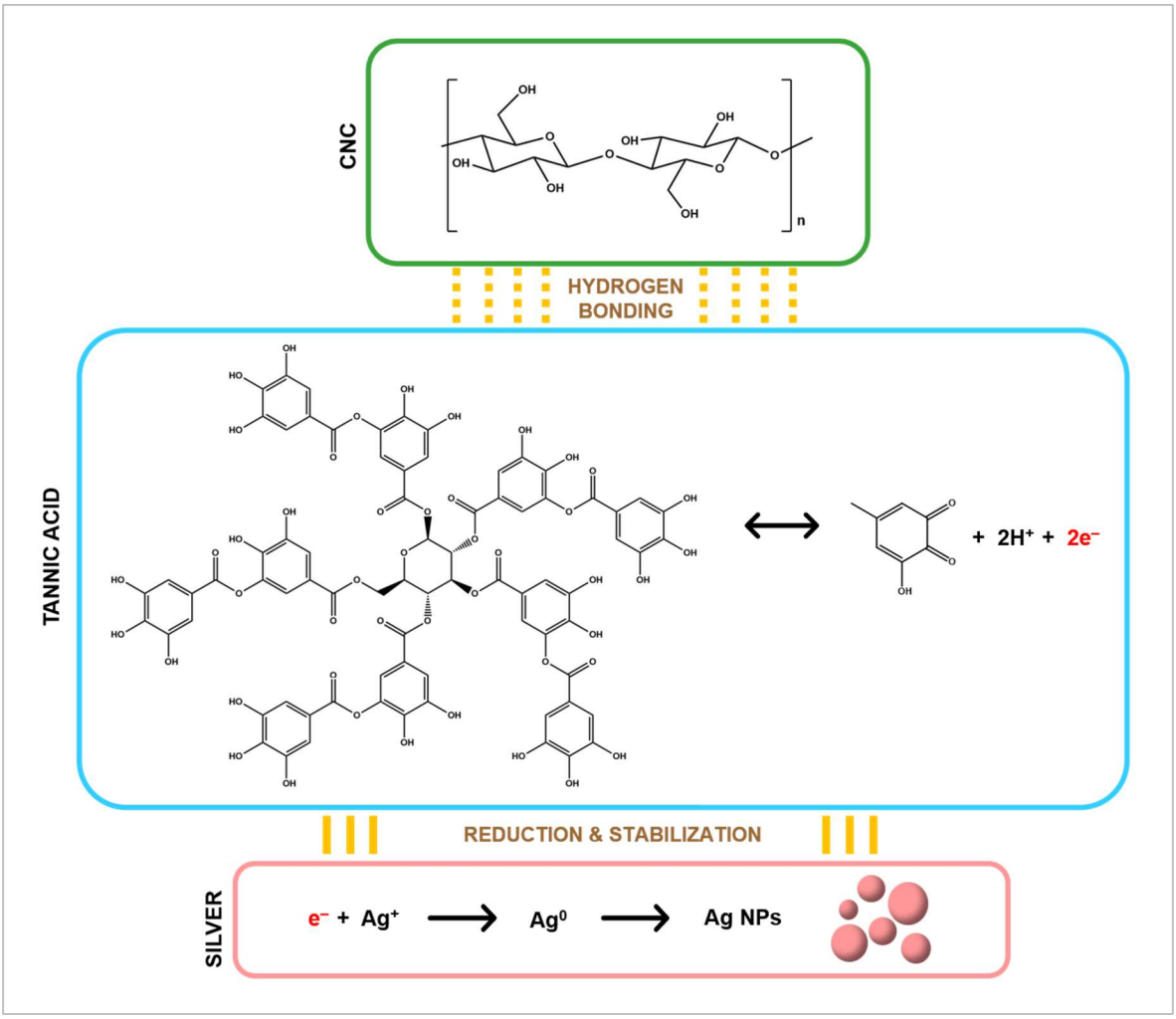

Figure 16: Synthesis route of CNC-TA-Ag nanofiller. CNC and TA in solution hydrogen bond together to form the coated CNC-TA. $AgNO_3$ is subsequently used to provide Ag^+ ions, to which TA donates electrons to induce the formation of Ag NPs.

more NPs attached than others. The zeta potential values (Table 5) of the CNC, CNC-TA, and CNC-TA-Ag all confirm that the modified CNC is stable after each synthesis step, as the potential is <|30| mV for the intermediate and final products.

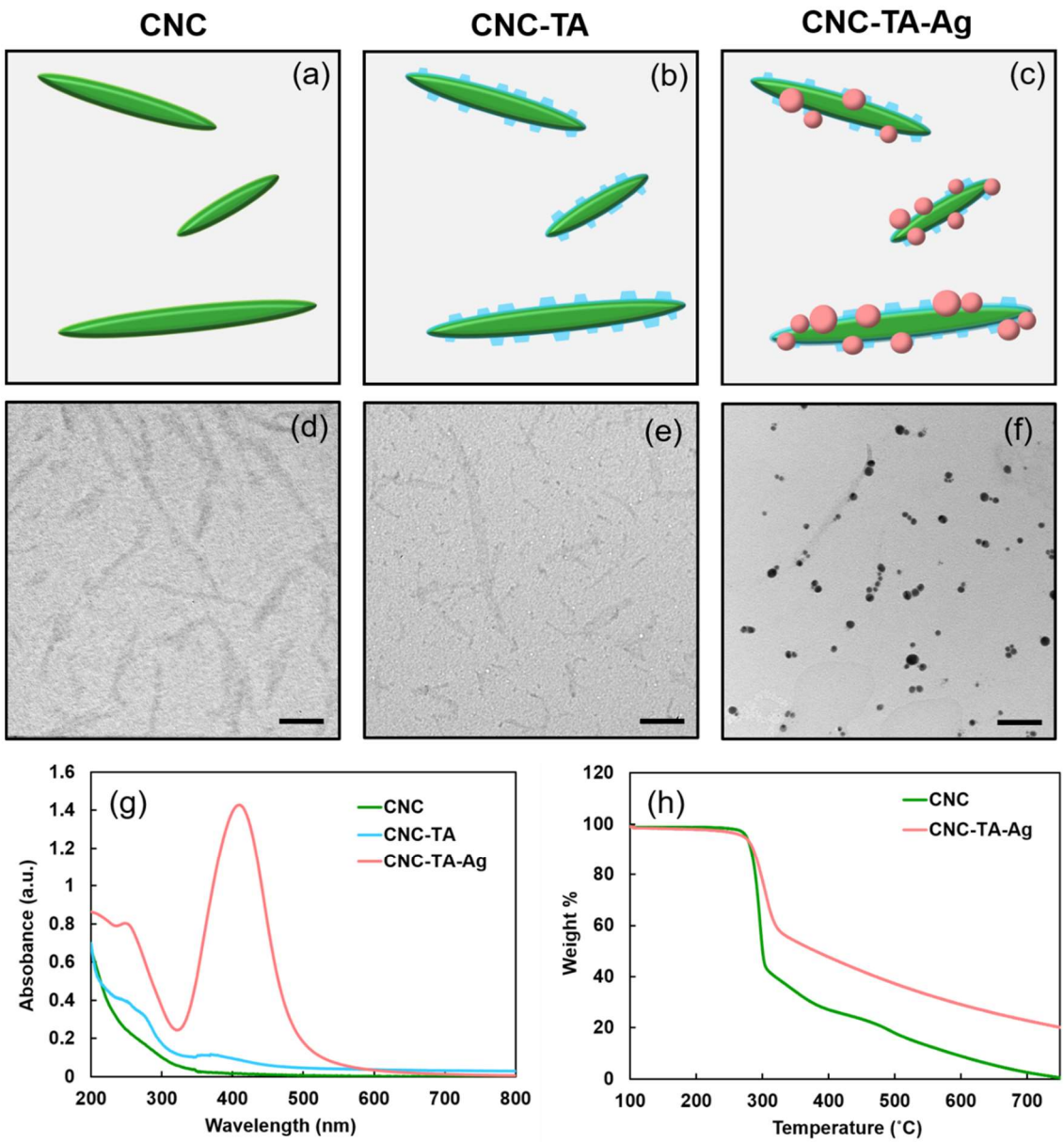

Figure 17: Visual depiction and TEM images of CNC (a, d), CNC-TA (b, e), and CNC-TA-Ag (c,f). The Ag NPs are clearly visible on the CNC substrate.

The CNC-TA-Ag product was further characterized using UV-vis spectroscopy, zeta potential, and TGA measurements. UV vis spectra (Figure 17g) for CNC-TA presented a peak at 210 and 276 nm, characteristic of the typical absorption peaks of TA[113]. The spectra for CNC-TA-Ag revealed a narrow Ag NP absorption peak around 410 nm, which indicates a blue

shift from the typical range of 420 – 450 nm for spherical silver NPs[114] due to the small particle size obtained.

The average quantity of silver synthesized on the CNC was determined using TGA. The degradation curve of neat CNC was compared to the modified CNC containing silver, where a 20 wt% difference was observable between the two after full decomposition of CNC at 750 °C (Figure 17h). As silver is not expected to melt until 962 °C, these remaining constituents were attributed to the Ag NPs synthesized on the CNC surface. The final CNC-TA-Ag product therefore contained 0.2 g silver/g CNC. The TGA curves also showed a slight increase in degradation temperature between the CNC and CNC-TA-Ag, rising from 286 °C to 300 °C for the respective samples. This is likely due to the TA-Ag coating slightly slowing decomposition of the CNC as it is exposed to heat.

Table 5: Zeta potential values of CNC, CNC-TA, and CNC-TA-Ag at pH 8.

Material	Zeta Potential (mV)
CNC	-37.8 ± 4.4
CNC-TA	-55.5 ± 3.2
CNC-TA-Ag	-47.1 ± 1.9

4.3.3 Antimicrobial properties of CNC-TA-Ag

MIC plate tests using CNC-TA-Ag revealed that the filler was effective against both Gram-negative (*E. coli*) and Gram-positive (*S. aureus*) strains of bacteria, with some plates shown in Figure 18a-j. Visually, the reduction in bacterial growth is evident for both species of bacteria after exposure to CNC-TA-Ag and the graphs of CFU reduction confirm this (Figure 18k). The full

MIC data, summarized in Table 6, indicated an affinity against *E. coli*. As observed from the chart, the MIC for CNC-TA-Ag against *E. coli* is 16 μg/mL. Accounting for the mass of antibacterial agent only, Ag NPs, this corresponds to only 3.2 μg/mL of silver required to inhibit bacterial growth.

Against *S. aureus*, the MIC of CNC-TA-Ag is 100 μg/mL corresponding to 20 μg/mL of silver. Evidently, the modified CNC was still effective against the Gram-positive bacteria, but posed a much larger threat against the Gram-negative strain. Potentially due to the differences in cell membrane composition[115,116], the Ag NPs required higher concentrations to inhibit bacterial growth for *S. aureus*. This Gram-positive strain contains a thick outer layer of peptidoglycan, while Gram-negative strains have an outer lipid membrane with only a thin peptidoglycan layer[116].

Other researchers also frequently reported higher sensitivity of Gram-negative bacteria to metal nanoparticles compared to Gram-positive[66,117,118], however it is possible that Gram stain may not be the sole cause for the difference in bacterial sensitivity. As the exact mechanism of antibacterial activity of metal nanoparticles is not fully understood, it is possible that other characteristics, such as the nanoparticle shape, crystal structure, or surface charge govern the dominant mechanism of activity against different types of bacteria[119–121], and this could play a role in the varied results obtained in this work for *E. coli* versus *S. aureus*.

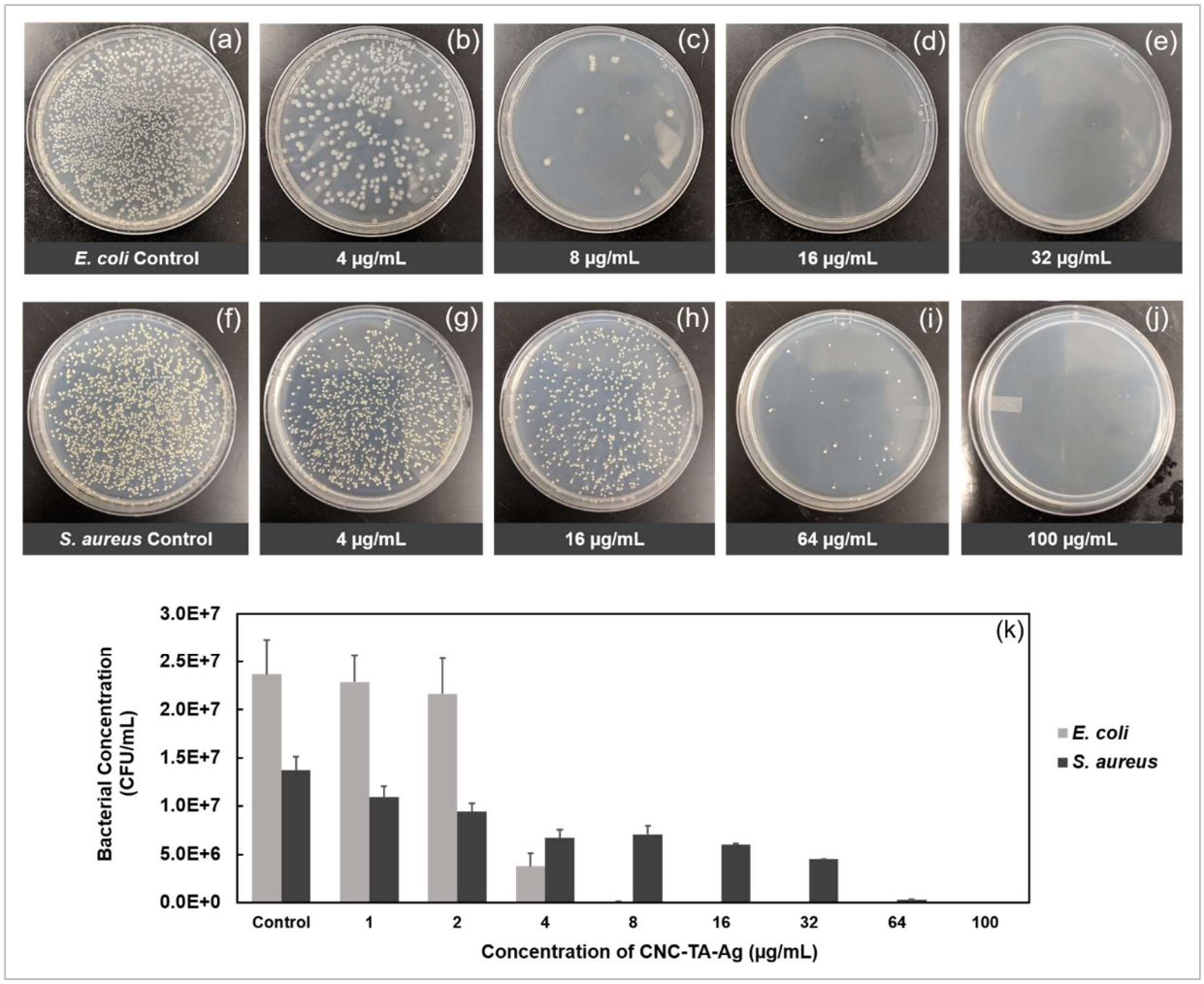

Figure 18: Antimicrobial activity of CNC-TA-Ag evaluated against E. coli (first row, a-e), and against S. aureus (second row, f-j). The plates are at 10 000X dilution, and visually show the reduction in bacterial growth with increasing concentrations of CNC-TA-Ag, where the concentrations are shown on the bottom of each plate. The calculated reduction in CFU count at each CNC-TA-Ag concentration is shown in (k).

Table 6: Percent reduction of bacterial populations treated with varying concentrations of CNC-TA-Ag to determine minimum inhibitory concentration (MIC).

Ag-TA-CNC Concentration (µg/mL)	**1**	**2**	**4**	**8**	**16**	**32**	**64**	**100**
% Reduction *E. coli*	16.72	17.57	81.48	99.64	99.99	100.00	100.00	100.00
% Reduction *S. aureus*	20.44	31.39	51.09	48.54	55.84	67.15	97.63	100.00

Comparing the obtained MICs to literature values for free Ag NPs of similar size, the CNC-stabilized Ag NPs in this study display lower MIC for bacterial growth. Agnihotri et al. reported MIC values of 30 and 100 µg Ag/mL for *E. coli* and *S. aureus* respectively, for Ag NPs with a size of approximately 15 nm[66]. This work indicated that for *E. coli,* the CNC-TA-Ag possessed an MIC of only 3.2 µg Ag/mL. The MIC for the CNC-TA-Ag against *S. aureus* was also found to be lower than the literature at 20 µg Ag/mL. This significant improvement in bacterial inhibition can be attributed to the stabilization of Ag NPs on CNC, whereas free floating Ag NPs often agglomerate in the absence of surfactants[122]. The CNC was therefore a very effective carrier for the metal nanoparticles in solution. Overall, the CNC-TA-Ag in this project was proven to be a useful antimicrobial material, where plate tests were able to show negligible microbial growth on the substrate and improved MIC compared to free Ag NPs.

4.3.4 Preliminary antimicrobial rubber tests

Preliminary antimicrobial tests were performed on neat rubber containing only CNC-TA-Ag, as a proof of concept to test the material for bactericidal activity. The hypothesis is whether the dipped nanocomposite films would be effective with the CNC-TA-Ag filler encapsulated in the rubber substrate, prior to optimization of the dipping formulation. For this test, 1 phr of CNC-TA-Ag was mixed into the neat NR without additives and casted to form a continuous film.

Using the same procedure for MIC tests, two replicates of plate tests were performed against Gram-negative *E. coli.* It was clear from the plates shown in Figure 19 that there was some reduction in bacterial growth using the rubber sample compared to the control, which was a good indicator of bactericidal activity of the films. Additional replicates are required to confirm this, as well as a comparison to Gram-positive bacteria such as *S. aureus* to test the versatility of the

material against various microbes. More rigorous testing of the rubber nanocomposite material will be a subject of further study using dipped NR and NBR films, including an additional control sample against NR and NBR with no CNC-TA-Ag filler loading.

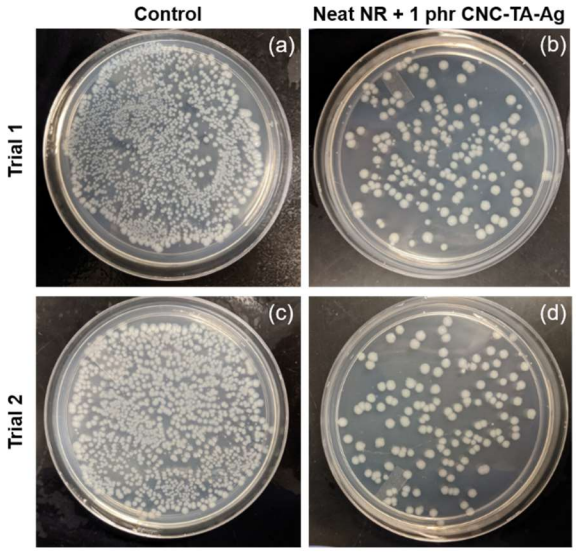

Figure 19: Preliminary results of bactericidal efficacy of neat NR films containing only 1 phr of CNC-TA-Ag and no additional additives. Plates are at 10 000X dilution.

4.3.5 Dipped nanocomposite rubber mechanical tests

Rubber films consisting of either NR or NBR and containing filler loading levels of 0.5, 1, or 3 phr of CNC-TA-Ag were prepared via coagulant dipping with the formulations in Table 2, Table 3, and

Table 4. The dipped films are denoted NR, NR0.5, NR1, NR3, NBR, NBR0.5, NBR1, and NBR3 (Figure 20) and were tested for their mechanical properties. These films were formulated to more accurately mimic industrial glove manufacturing methods, to determine if the formulation was suitable when prepared with the necessary additives for rubber film processing and subject to

similar assembly parameters. Due to the directional movement of dipping, samples were cut parallel and normal to the dip direction to test and determine any anisotropy of the material.

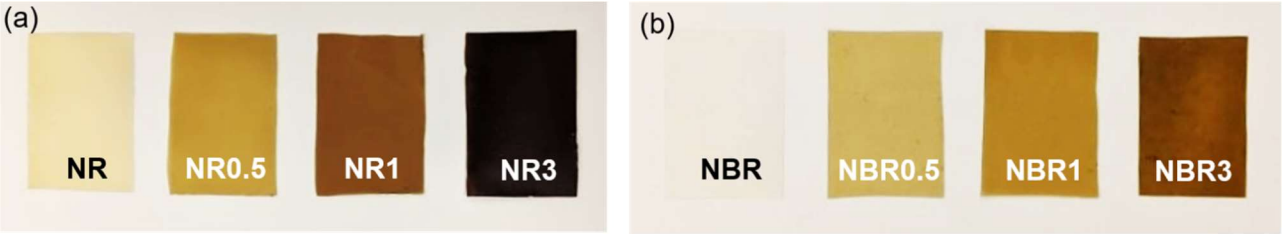

Figure 20: Coagulant dipped NR and NBR films containing varying loading levels of CNC-TA-Ag.

Figure 21 shows the tensile results for NR films and Figure 22 summarizes the results from NBR films, including typical stress-strain curves for the materials. As expected with rigid filler additives[123], the elastic moduli of the NR and NBR composites increased proportionally to the increase in filler loading level. Higher CNC-TA-Ag loading increased the polymer stiffness, where the material was able to resist greater applied force prior to permanent plastic deformation. The ultimate tensile strength (UTS) of the materials were also expected to increase, though it was observed from the typical stress-strain curves that the UTS was highly dependent on the elongation of the material. For both NR and NBR, the trends observed in strength are mirrored in the trends for elongation, which suggests a strong correlation between the two due to the property of rubbers to exhibit strain hardening but no necking prior to fracture[124].

In NR, the strength and elongation of the films are observed to increase from neat NR to NR0.5, then subsequently decreased for NR1 and NR3. This increase in UTS and elongation is also observed for NBR films for the loading levels of NBR0.5 and NBR1, followed by a decrease in both for NBR3. The initial increases in strength can be attributed to the modified CNC filler

inducing strain hardening at lower strain levels within the NR samples. Due to the presence of rigid filler within the entangled polymer matrix, greater force is required to stretch the rubber

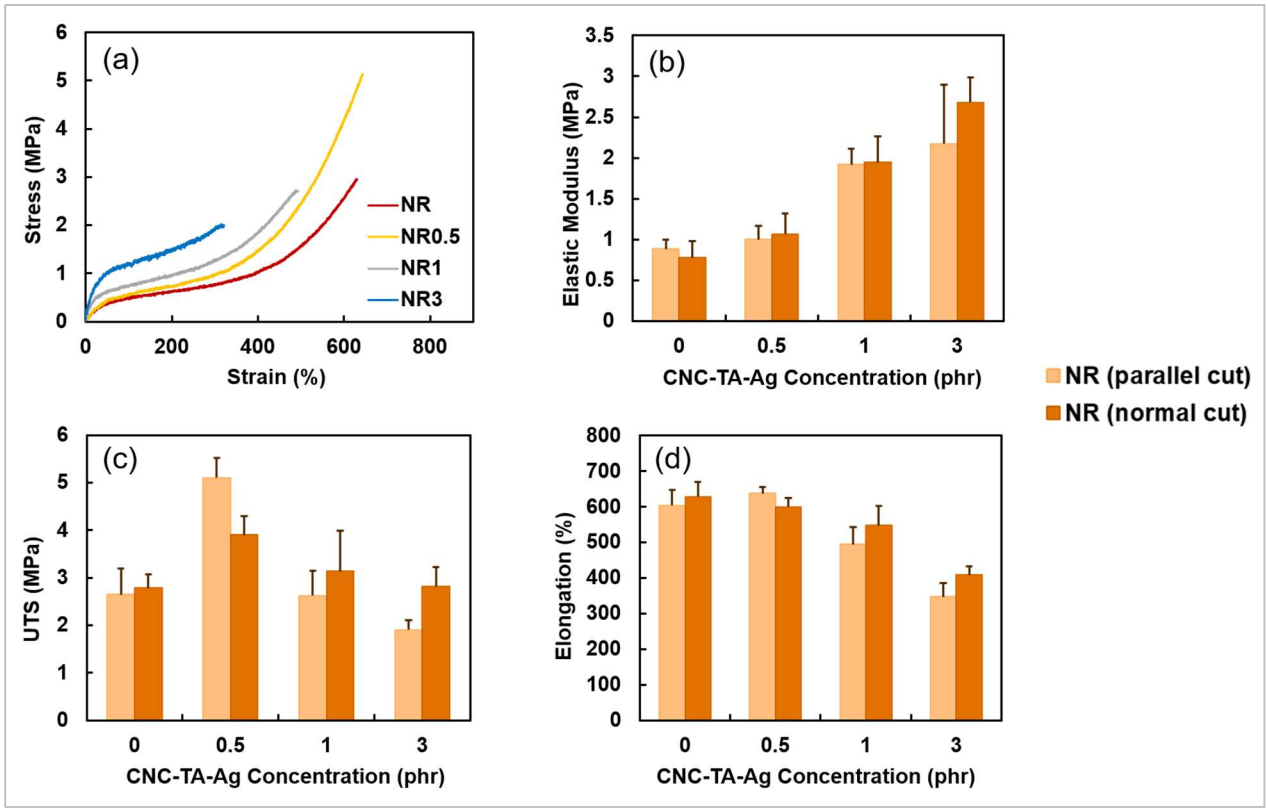

Figure 21: Tensile test results for NR nanocomposites with increasing CNC-TA-Ag loading. Typical stress-strain curves for parallel cut samples are shown in (a), and the average elastic modulus (b), ultimate tensile strength (UTS) (c), and elongation (d) for parallel and normal cut NR samples are compared.

chains and therefore yields greater tensile strength. However, high amounts of nanofillers can significantly restrict polymer chain mobility and are therefore expected to decrease elongation[125]. These two opposing factors lead to initial increases in elongation and strength, followed by decreases in both as the polymer chain mobility becomes significantly restricted.

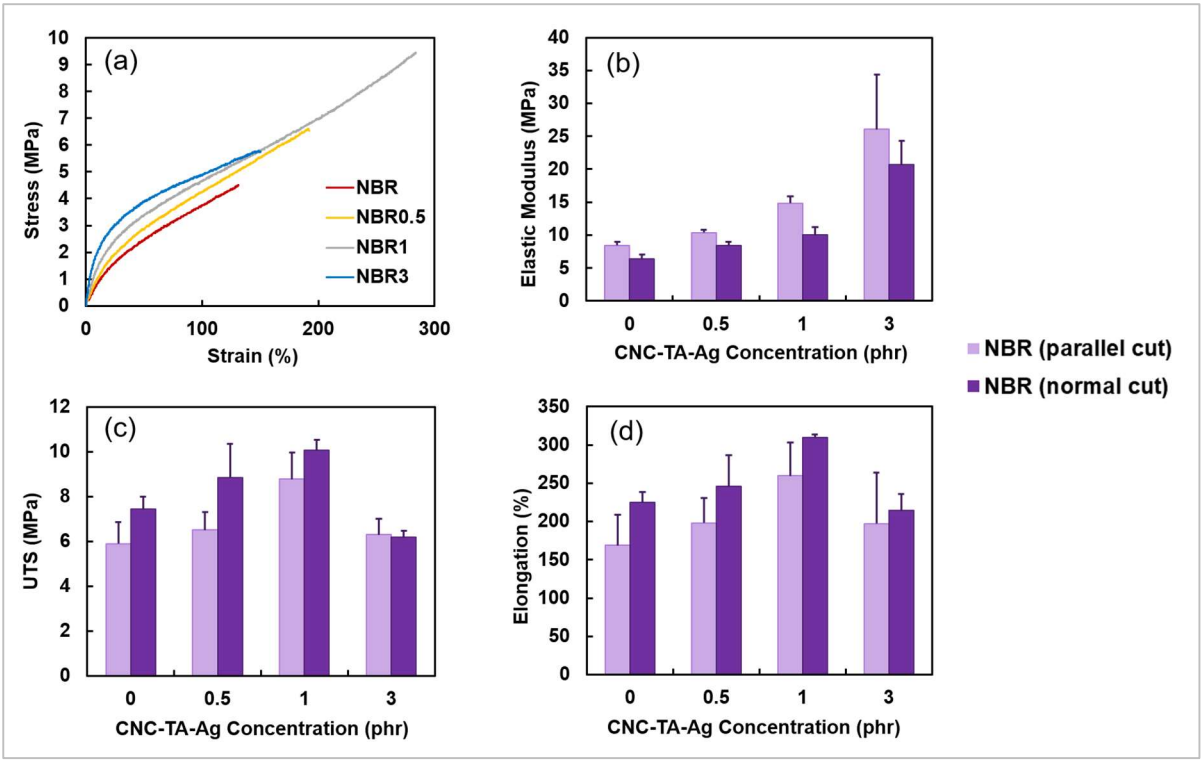

Figure 22: Tensile test results for NBR nanocomposites with increasing CNC-TA-Ag loading. Typical stress-strain curves for parallel cut samples are shown in (a), and the average elastic modulus (b), ultimate tensile strength (UTS) (c), and elongation (d) for parallel and normal cut NBR samples are compared.

Comparing the parallel and normal cut samples for both NR and NBR, the differences observed from the data were not substantial. It was expected that any isotropy would lead to polymer chain and CNC alignment with the dip direction, thus the parallel samples were hypothesized to yield larger improvements in modulus, elongation, and strength. Accounting for the standard deviation on the graphs, however, it is evident that there is minimal to no alignment present in the films. The parallel cut NR samples had statistically no difference in modulus, strength, and elongation compared to the normal cut samples. For NBR samples, the moduli of parallel cut specimens were slightly higher than the normal cut, indicating some grain structure, but the strength and elongation were observed to be approximately the same. This lack of

anisotropy can be attributed to the low viscosity of the latex dip mixture, thus forcing no chain or CNC alignment during the dipped film preparation.

Since the tensile test results revealed that the samples were isotropic, Type T tear samples were prepared only parallel to the grain as per ASTM specifications for tear strength. The tear strength results (Figure 23) indicate that the CNC-TA-Ag aided in enhancing the material resistance to tear propagation. Due to increasing tortuosity in the films, cracks required more applied force to persist through the material. In alignment with previous results from our group[126], there was a jump in the tear force at 3 phr. Based on the aspect ratio of CNC used in this project, the percolation threshold of the filler was determined to be approximately 2.9 phr[126], and this network of interconnected filler in NR3 and NBR3 samples resulted in the highest tear resistance due to the complex path of crack propagation. These results confirm that the CNC-TA-Ag filler are useful for improving the strength and durability of NR and NBR thin films.

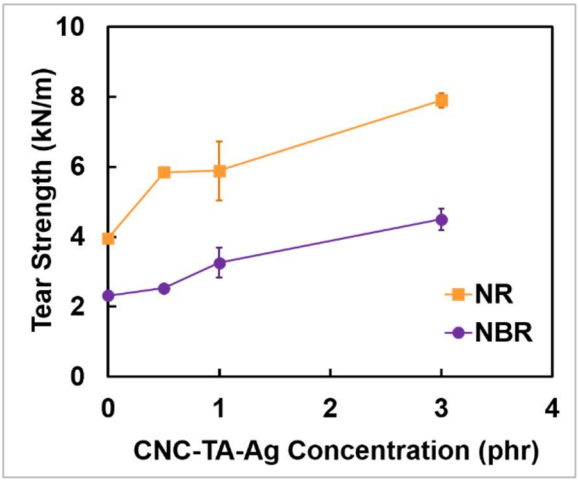

Figure 23: Tear test results for NR and NBR nanocomposite films. Increasing tear strength is observed with increasing concentrations of CNC-TA-Ag incorporated into the rubber matrices.

4.4 Future Work & Conclusions

A multifunctional filler material was prepared by modifying the CNC with Ag NPs via green synthesis methods. This modified CNC was used to strengthen and reinforce rubber thin films, where the dipped rubber films investigated in this study were shown to display increased modulus and tear strength with the addition of CNC-TA-Ag filler. In addition, the CNC-TA-Ag was shown to be bactericidal both on its own and within a neat NR matrix. The next steps are to test dipped NR and NBR films for their antimicrobial efficacy with more rigorous trials. The NR and NBR nanocomposites could have applications in the medical field for surgical gloves, or in food handling environments to prevent transfer of bacteria between uncooked foods.

This project presents several advantages in the design and execution of the nanocomposite material produced. First, Ag NPs are more versatile for combatting different types of infections due to the various ways in which they can inactivate bacterial cells. Second, the attachment of Ag NPs onto CNC prevents aggregation, which is a common problem encountered with metal NPs. Since CNC is used as a Ag NP carrier, the CNC-TA-Ag is capable of providing both strength and antibacterial functionality. CNC-TA-Ag can therefore also be used as an active antimicrobial ingredient for other applications and materials, such as bandages or surface coatings that require high sterility. The work performed here provides a detailed starting point for antimicrobial nanocomposites that can be used in various industrial applications.

4.5 Supplementary Information

The optimization of the CNC-TA-Ag synthesis was performed by investigating different pHs and molar ratios of TA:Ag. Characterization of the CNC-TA-Ag product was then conducted using UV-vis and zeta potential. The most effective synthesis parameters were selected for the final CNC-TA-Ag filler preparation method, as outlined above.

The effectiveness of TA for Ag NP synthesis was first investigated at varying pHs. For this pH study, 500 mL of 1 wt% CNC dispersion was prepared, and 1.2 g HEPES buffer was added. The dispersion was then separated into five 100 mL batches, which were adjusted to pH 4, 6, 7, 8, and 10. TA (0.1 g in 4 mL DI water) was added to each batch and allowed to react for 18 hours at room temperature. After reaction, the pH of each batch was checked and re-adjusted to the desired value. Enough $AgNO_3$ solution (2.5 mg/mL) was added to each batch to give a 1:2 molar ratio of TA:Ag. Dialysis was then performed on the final solution for four days against DI water, and one day against miliQ water. The samples were diluted to 0.1 mg/mL solid content and analyzed under UV-vis and zeta potential as per Figure S1.

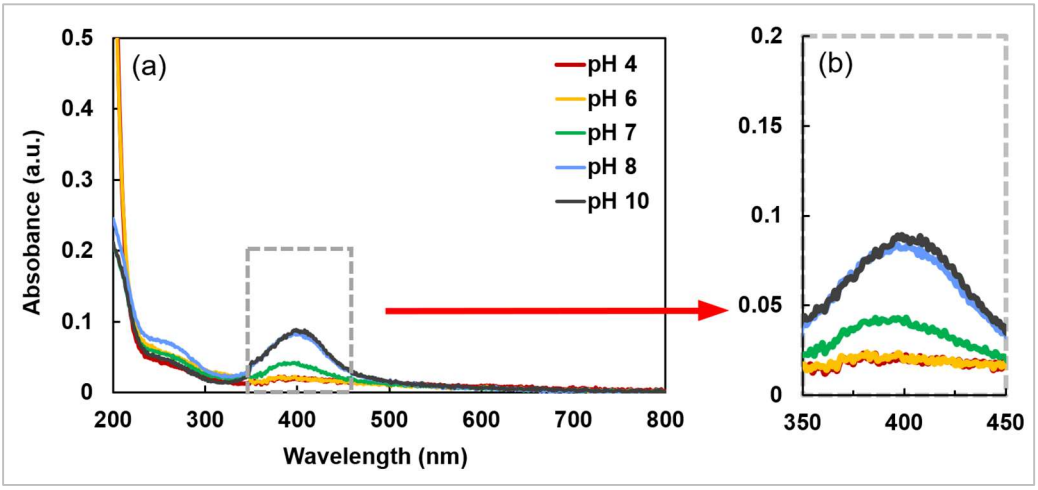

Figure S1: UV-vis spectra of CNC-TA-Ag using varying pH

It is evident from the UV-vis data that the highest silver NP peaks were obtained at pH 8 and pH 10. Comparing these two peaks in the enlarged graph (Figure S1b), the peak magnitudes are very close to one another, showing the highest pH (10) was only marginally more effective at synthesizing more silver NP compared to the second highest pH (8). In contrast, a significant increase in absorbance is seen from pH 6 to pH 7, and finally pH 8. This result supports the literature, indicating only mildly basic or acidic conditions significantly affect the ability of TA to act as a reducing and capping agent. Since the pKa of TA is approximately 6, pH values above this lend to more effective reduction of silver ions due to the increased presence of protons in solution.

As pH 8 was very effective for silver NP synthesis, it was used for further experiments to determine the best molar ratio (MR) of TA:Ag. Using the same method as the pH study, MR of 1:0.65, 1:1, 1:2, and 1:20 were tested. Literature from Sivaraman et al. indicates that lower ratios of Ag can lead to slower reduction onto the TA and thus create larger silver NPs[127], while smaller silver NPs are deemed more effective for antimicrobial activity[64]. The purpose of the CNC-TA-Ag in this project is to act as a reinforcing filler when incorporated into a rubber matrix, thus a large quantity of silver NPs with small diameter was desired on the CNC. The influence of MR on the final CNC-TA-Ag product was studied with UV-vis, with samples diluted to 0.1 mg/mL (Figure S2).

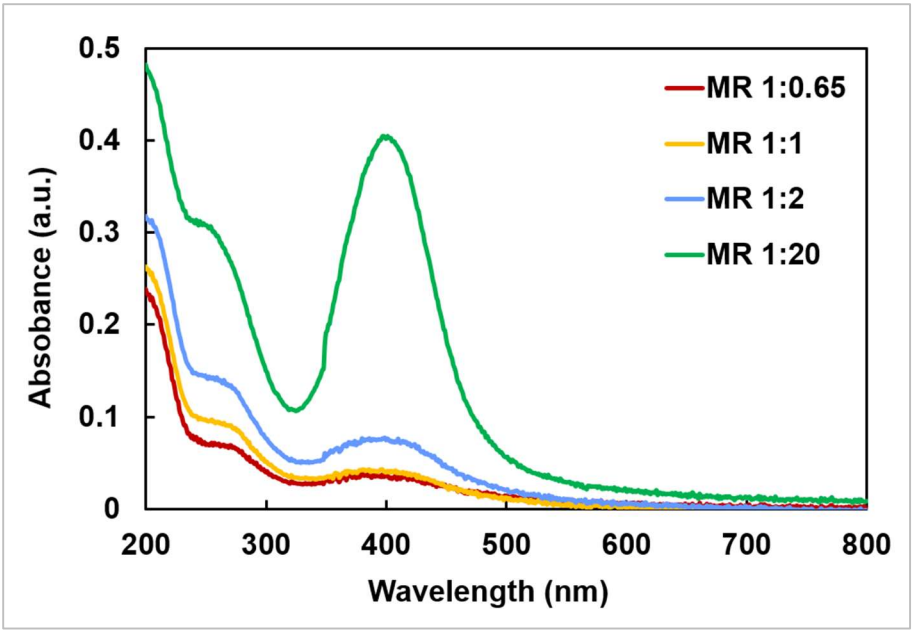

Figure S2: UV-vis spectra of CNC-TA-Ag using varying molar ratio (MR) of TA:Ag

The MR UV-vis curves reveal that a ratio of 1:20 of TA:Ag yielded the highest silver NP peak, indicating significantly more silver NP production on the CNC compared to other ratios. This was attributed to the ability of one TA molecule to donate 20 electrons in solution, thus exploiting its full ability as a reducing agent. The final parameters used in the final CNC-TA-Ag synthesis were therefore pH 8 and MR 1:20.

The stability of all iterations of CNC-TA-Ag synthesis were analyzed with zeta potential, as per Table S1. It was observed that the final product obtained from all methods were very stable, with an absolute zeta potential value of > 30 mV. The CNC was hence very effective as a carrier for Ag NPs to prevent aggregation in solution.

Table S1: Zeta potential of CNC-TA-Ag synthesized with varying pH and molar ratios.

Material	Trial	Zeta Potential (mV)
CNC-TA-Ag	pH 4	-39.1 ± 1.7
	pH 6	-38.4 ± 2.1
	pH 7	-37.5 ± 3.7
	pH 8	-46.5 ± 2.2
	pH 10	-46.0 ± 1.5
	MR 1:0.65	-44.6 ± 1.0
	MR 1:1	-44.6 ± 0.9
	MR 1:2	-45.7 ± 1.2
	MR 1:20	-45.9 ± 1.2

CHAPTER 5

Concluding remarks

The necessity of producing fully renewable, sustainable, and biodegradable materials is a monumental challenge that humans face. As worldwide waste increases, polymer products of all types are found undegraded in the environment, polluting various regions of the earth. Hence, this thesis has focused on the use of green chemistry and renewable feedstocks for the synthesis of enhanced rubber nanocomposites.

CNC, obtained from cellulose biomass, possesses excellent filler properties such as high aspect ratio and high tensile strength due to its high rigidity. Its abundant surface hydroxyl groups yield a high potential for modifications and allow for ease of dispersion in aqueous media. This work first used colloidal CNC to evaluate its baseline reinforcing properties on rubber thin sheets, then subsequently modified the CNC to carry antimicrobial Ag NPs.

Pristine CNC in this research was incorporated up to loading levels of 8 phr within thin sheets of NR and SBR. Above the percolation threshold of 2.9 phr, CNC was seen to yield significantly enhanced tear properties and tensile properties. The trend in water permeability and absorption by the films also increased after a continuous CNC filler network was formed. The considerable improvement of CNC on tear strength could facilitate the production of extremely thin rubber sheets for high touch sensitivity and high durability.

Antimicrobial modifications to CNC were achieved by the addition of TA to the surface, interacting with CNC via electrostatic interactions. Using alkaline pH to reduce TA into gallic acid and glucose units, Ag NPs were grown *in situ* on the surface of the CNC-TA complex to a size of approximately 15 nm. Characterization of the CNC-TA-Ag product confirmed successful synthesis with TEM imaging and UV-vis spectroscopy, and TGA analysis indicated a silver loading level of approximately 20 wt% CNC. Bacterial tests on the CNC-TA-Ag proved the

material was effective against both *E. coli* and *S. aureus*. MIC values of 3.2 µg Ag/mL and 20 µg Ag/mL were achieved for the Gram-negative and Gram-positive strain, respectively.

CNC-TA-Ag was incorporated into dipped NR and NBR films to create antimicrobial rubber nanocomposites. Again, tensile and tear properties of the films were improved with the modified CNC addition. Preliminary antibacterial tests on neat NR with 1 phr of CNC-TA-Ag showed a significant reduction in bacterial growth after contact with the rubber. The film formulations show great potential for industrial thin film products, such as gloves, and the CNC-TA-Ag on its own may be used for other types of nanocomposites for enhanced mechanical properties and antibacterial attributes. Further testing on CNC-TA-Ag composites may be done for more rigorous antibacterial studies, biodegradability, and functionality in different materials to increase its breadth of opportunity as an advanced green functional filler. The CNC-stabilized Ag NPs may open many new avenues for antimicrobial product development.

REFERENCES

1. Mülhaupt, R. Green polymer chemistry and bio-based plastics: dreams and reality. *Macromol. Chem. Phys.* **214**, 159–174 (2013).

2. Papageorgiou, G. Thinking green: sustainable polymers from renewable resources. *Polymers (Basel).* **10**, 952 (2018).

3. Mülhaupt, R. Hermann Staudinger and the origin of macromolecular chemistry. *Angew. Chemie Int. Ed.* **43**, 1054–1063 (2004).

4. Williams, C. & Hillmyer, M. Polymers from renewable resources: a perspective for a special issue of Polymer Reviews. *Polym. Rev.* **48**, 1–10 (2008).

5. Geyer, R., Jambeck, J. R. & Law, K. L. Production, use, and fate of all plastics ever made. *Sci. Adv.* **3**, e1700782 (2017).

6. Law, K. L. Plastics in the marine environment. *Annual Review of Marine Science* **9**, 205–229 (2017).

7. Jamieson, A. J. *et al.* Microplastics and synthetic particles ingested by deep-sea amphipods in six of the deepest marine ecosystems on Earth. *R. Soc. Open Sci.* **6**, 180667 (2019).

8. US Environmental Protection Agency & Office of Resource Conservation and Recovery. Basic Information | Scrap Tires. Available at: https://archive.epa.gov/epawaste/conserve/materials/tires/web/html/basic.html. (Accessed: 10th January 2020)

9. Czuppon, A. B. *et al.* The rubber elongation factor of rubber trees (Hevea brasiliensis) is the major allergen in latex. *J. Allergy Clin. Immunol.* **92**, 690–697 (1993).

10. Rose, K. & Steinbüchel, A. Biodegradation of natural rubber and related compounds: recent insights into a hardly understood catabolic capability of microorganisms. *Appl. Environ. Microbiol.* **71**, 2803–2812 (2005).

11. Zhu, Y., Romain, C. & Williams, C. K. Sustainable polymers from renewable resources. *Nature* **540**, 354–362 (2016).

12. Mark, J. E. *Polymer Data Handbook*. (Oxford University Press, 2009).

13. Keddie, J. L. & Routh, A. F. *Fundamentals of Latex Film Formation*. (Springer, 2010).

14. Zhang, R. Cis-1,2-polyisoprene. in *Polymer Data Handbook* (ed. Mark, J. E.) 607–619 (Oxford University Press, 1999). doi:10.1081/e-ebpp-120051909

15. Singh, M. & Lim, H. M. E. *Surfactants and their Use in Latex Technology*. *Malaysian Rubber Board: Rubber Technology Developments* **13**, (2013).

16. Akiba, M. & Hashim, A. S. Vulcanization and crosslinking in elastomers. *Prog. Polym. Sci.* **22**, 475–521 (1997).

17. Yasuda, Y., Minoda, S., Ohashi, T., Yokohama, H. & Ikeda, Y. Two-phase network formation in sulfur crosslinking reaction of isoprene rubber. *Macromol. Chem. Phys.* **215**, 971–977 (2014).

18. Ogunsona, E., Hojabr, S., Berry, R. & Mekonnen, T. H. Nanocellulose-triggered structural and property changes of acrylonitrile-butadiene rubber films. *Int. J. Biol. Macromol.* (2020). doi:10.1016/j.ijbiomac.2020.07.202

19. Ikeda, Y. *et al.* Dinuclear bridging bidentate zinc/stearate complex in sulfur cross-linking of rubber. *Macromolecules* **48**, 462–475 (2015).

20. Liu, M. & Horrocks, A. R. Effect of carbon black on UV stability of LLDPE films under artificial weathering conditions. *Polym. Degrad. Stab.* **75**, 485–499 (2002).

21. Yousif, E. & Haddad, R. Photodegradation and photostabilization of polymers, especially polystyrene: review. *Springerplus* **2**, 398 (2013).

22. Sharif Sh., M., Golestani Fard, F., Khatibi, E. & Sarpoolaky, H. Dispersion and stability of carbon black nanoparticles, studied by ultraviolet–visible spectroscopy. *J. Taiwan Inst. Chem. Eng.* **40**, 524–527 (2009).

23. Pourhossaini, M.-R. & Razzaghi-Kashani, M. Effect of silica particle size on chain dynamics and frictional properties of styrene butadiene rubber nano and micro composites. *Polymer (Guildf).* **55**, 2279–2284 (2014).

24. Fragiadakis, D., Bokobza, L. & Pissis, P. Dynamics near the filler surface in natural rubber-silica nanocomposites. *Polymer (Guildf).* **52**, 3175–3182 (2011).

25. Peng, C.-C., Göpfert, A., Drechsler, M. & Abetz, V. "Smart" silica-rubber nanocomposites in virtue of hydrogen bonding interaction. *Polym. Adv. Technol.* **16**, 770–782 (2005).

26. Hentschke, R. The Payne effect revisited. *Express Polym. Lett.* **11**, 278–292 (2017).

27. Meera, A. P., Said, S., Grohens, Y. & Thomas, S. Nonlinear viscoelastic behavior of silica-filled natural rubber nanocomposites. *J. Phys. Chem. C* **113**, 17997–18002 (2009).

28. Praveen, S. *et al.* Synergistic effect of carbon black and nanoclay fillers in styrene butadiene rubber matrix: development of dual structure. *Compos. Part A Appl. Sci. Manuf.* **40**, 309–316 (2009).

29. Qu, L. *et al.* Synergistic reinforcement of nanoclay and carbon black in natural rubber. *Polym. Int.* **59**, 1397–1402 (2010).

30. Suriani, A. B., Nurhafizah, M. D., Mohamed, A., Zainol, I. & Masrom, A. K. A facile one-step method for graphene oxide/natural rubber latex nanocomposite production for supercapacitor applications. *Mater. Lett.* **161**, 665–668 (2015).

31. Matos, C. F., Galembeck, F. & Zarbin, A. J. G. Multifunctional and environmentally friendly nanocomposites between natural rubber and graphene or graphene oxide. *Carbon N. Y.* **78**, 469–479 (2014).

32. Shang, S., Gan, L., Yuen, M. C., Jiang, S. & Mei Luo, N. Carbon nanotubes based high temperature vulcanized silicone rubber nanocomposite with excellent elasticity and electrical properties. *Compos. Part A Appl. Sci. Manuf.* **66**, 135–141 (2014).

33. Selvan, N. T. *et al.* Piezoresistive natural rubber-multiwall carbon nanotube nanocomposite for sensor applications. *Sensors Actuators A Phys.* **239**, 102–113 (2016).

34. Gomez, C. V. *et al.* Structural and electronic properties of graphene oxide for different degree of oxidation. *Mater. Today Proc.* **3**, 796–802 (2016).

35. Dong, S., Bortner, M. J. & Roman, M. Analysis of the sulfuric acid hydrolysis of wood pulp for cellulose nanocrystal production: a central composite design study. *Ind. Crops Prod.* **93**, 76–87 (2016).

36. Kumar, A., Negi, Y. S., Choudhary, V. & Bhardwaj, N. K. Characterization of cellulose nanocrystals produced by acid-hydrolysis from sugarcane bagasse as agro-waste. *J. Mater. Phys. Chem.* **2**, 1–8 (2014).

37. Grishkewich, N., Mohammed, N., Tang, J. & Tam, K. C. Recent advances in the application of cellulose nanocrystals. *Curr. Opin. Colloid Interface Sci.* **29**, 32–45 (2017).

38. Martin-Martinez, F. J. Designing nanocellulose materials from the molecular scale. *Proc. Natl. Acad. Sci.* **115**, 7174–7175 (2018).

39. Islam, M. S., Chen, L., Sisler, J. & Tam, K. C. Cellulose nanocrystal (CNC)–inorganic hybrid systems: synthesis, properties and applications. *J. Mater. Chem. B* **6**, 864–883 (2018).

40. Wu, X., Moon, R. J. & Martini, A. Crystalline cellulose elastic modulus predicted by atomistic models of uniform deformation and nanoscale indentation. *Cellulose* **20**, 43–55 (2013).

41. CelluForce Inc. NanoCrystalline Cellulose applications | CelluForce. (2016). Available at: https://www.celluforce.com/en/markets/. (Accessed: 20th February 2020)

42. Chen, Y., Zhang, Y., Xu, C. & Cao, X. Cellulose nanocrystals reinforced foamed nitrile rubber nanocomposites. *Carbohydr. Polym.* **130**, 149–154 (2015).

43. Tian, M. *et al.* Bioderived rubber-cellulose nanocrystal composites with tunable water-responsive adaptive mechanical behavior. *ACS Appl. Mater. Interfaces* **9**, 6482–6487 (2017).

44. Dhar, P., Bhardwaj, U., Kumar, A. & Katiyar, V. Poly(3-hydroxybutyrate)/cellulose nanocrystal films for food packaging applications: barrier and migration studies. *Polym. Eng. Sci.* **55**, 2388–2395 (2015).

45. Cranston, E. & Hu, Z. Surface modification of cellulose nanocrystals. *CA2895292A1* (2015).

46. Zhang, Z., Sèbe, G., Wang, X. & Tam, K. C. UV-Absorbing Cellulose Nanocrystals as Functional Reinforcing Fillers in Poly(vinyl chloride) Films. *ACS Appl. Nano Mater.* **1**, 632–641 (2018).

47. Dhar, P., Kumar, A. & Katiyar, V. Fabrication of cellulose nanocrystal supported stable Fe(0) nanoparticles: a sustainable catalyst for dye reduction, organic conversion and chemo-magnetic propulsion. *Cellulose* **22**, 3755–3771 (2015).

48. Samir, M. A. S. A., Alloin, F. & Dufresne, A. Review of recent research into cellulosic whiskers, their properties and their application in nanocomposite field. *Biomacromolecules* **6**, 612–626 (2005).

49. Eslami, H., Tzoganakis, C. & Mekonnen, T. H. Constructing pristine and modified cellulose nanocrystals based cured polychloroprene nanocomposite films for dipped goods application. *Compos. Part C Open Access* **1**, 100009 (2020).

50. de Castro, D. O., Bras, J., Gandini, A. & Belgacem, N. Surface grafting of cellulose nanocrystals with natural antimicrobial rosin mixture using a green process. *Carbohydr. Polym.* **137**, 1–8 (2016).

51. Sipponen, A. & Laitinen, K. Antimicrobial properties of natural coniferous rosin in the European Pharmacopoeia challenge test. *APMIS* **119**, 720–724 (2011).

52. Yu, H.-Y., Chen, G.-Y., Wang, Y.-B. & Yao, J.-M. A facile one-pot route for preparing cellulose nanocrystal/zinc oxide nanohybrids with high antibacterial and photocatalytic activity. *Cellulose* **22**, 261–273 (2015).

53. Pasquet, J. *et al.* The contribution of zinc ions to the antimicrobial activity of zinc oxide. *Colloids Surfaces A Physicochem. Eng. Asp.* **457**, 263–274 (2014).

54. Shi, Z. *et al.* Enhanced colloidal stability and antibacterial performance of silver nanoparticles/cellulose nanocrystal hybrids. *J. Mater. Chem. B* **3**, 603–611 (2015).

55. Neu, H. C. The crisis in antibiotic resistance. *Science (80-.).* **257**, 1064–1073 (1992).

56. Barillo, D. J. & Marx, D. E. Silver in medicine: a brief history BC 335 to present. *Burns* **40**, S3–S8 (2014).

57. McCue, R. W., McDougal, F. G. & Shay, D. E. The antibacterial properties of some dental restorative materials. *Oral Surgery, Oral Med. Oral Pathol.* **4**, 1180–1184 (1951).

58. Inkinen, J., Mäkinen, R., Keinänen-Toivola, M. M., Nordström, K. & Ahonen, M. Copper as an antibacterial material in different facilities. *Lett. Appl. Microbiol.* **64**, 19–26 (2017).

59. Pareek, V., Bhargava, A., Gupta, R., Jain, N. & Panwar, J. Synthesis and applications of noble metal nanoparticles: a review. *Adv. Sci. Eng. Med.* **9**, 527–544 (2017).

60. Singh, J. *et al.* 'Green' synthesis of metals and their oxide nanoparticles: applications for environmental remediation. *J. Nanobiotechnology* **16**, 84–107 (2018).

61. Vikas, S., Krishan, K. S. & Manjit, K. S. Nanosilver: potent antimicrobial agent and its biosynthesis. *African J. Biotechnol.* **13**, 546–554 (2014).

62. Thanh, N. T. K., Maclean, N. & Mahiddine, S. Mechanisms of nucleation and growth of nanoparticles in solution. *Chemical Reviews* **114**, 7610–7630 (2014).

63. Majeed Khan, M. A., Kumar, S., Ahamed, M., Alrokayan, S. A. & AlSalhi, M. S. Structural and thermal studies of silver nanoparticles and electrical transport study of their thin films. *Nanoscale Res. Lett.* **6**, 434 (2011).

64. Yi, Z. *et al.* Green, effective chemical route for the synthesis of silver nanoplates in tannic acid aqueous solution. *Colloids Surfaces A Physicochem. Eng. Asp.* **392**, 131–136 (2011).

65. Prabhu, S. & Poulose, E. K. Silver nanoparticles: mechanism of antimicrobial action, synthesis, medical applications, and toxicity effects. *Int. Nano Lett.* **2**, 32 (2012).

66. Agnihotri, S., Mukherji, S. & Mukherji, S. Size-controlled silver nanoparticles synthesized over the range 5–100 nm using the same protocol and their antibacterial efficacy. *RSC Adv.* **4**, 3974–3983 (2014).

67. Li, H., Chen, Q., Zhao, J. & Urmila, K. Enhancing the antimicrobial activity of natural extraction using the synthetic ultrasmall metal nanoparticles. *Sci. Rep.* **5**, 11033 (2015).

68. Stoimenov, P. K., Klinger, R. L., Marchin, G. L. & Klabunde, K. J. Metal oxide nanoparticles as bactericidal agents. *Langmuir* **18**, 6679–6686 (2002).

69. Sondi, I. & Salopek-Sondi, B. Silver nanoparticles as antimicrobial agent: a case study on E. coli as a model for Gram-negative bacteria. *J. Colloid Interface Sci.* **275**, 177–182 (2004).

70. Dibrov, P., Dzioba, J., Gosink, K. K. & Häse, C. C. Chemiosmotic Mechanism of Antimicrobial Activity of Ag+ in Vibrio cholerae. *Antimicrob. Agents Chemother.* **46**, 2668–2670 (2002).

71. Li, W.-R. *et al.* Antibacterial activity and mechanism of silver nanoparticles on Escherichia coli. *Appl. Microbiol. Biotechnol.* **85**, 1115–1122 (2010).

72. Feng, Q. L. *et al.* A mechanistic study of the antibacterial effect of silver ions on Escherichia coli and Staphylococcus aureus. *J. Biomed. Mater. Res.* **52**, 662–668 (2000).

73. Wong, K. K. Y. & Liu, X. Silver nanoparticles—the real "silver bullet" in clinical medicine? *Medchemcomm* **1**, 125–131 (2010).

74. Rai, M., Yadav, A. & Gade, A. Silver nanoparticles as a new generation of antimicrobials. *Biotechnol. Adv.* **27**, 76–83 (2009).

75. Boonkaew, B., Kempf, M., Kimble, R., Supaphol, P. & Cuttle, L. Antimicrobial efficacy of a novel silver hydrogel dressing compared to two common silver burn wound dressings: Acticoat™ and PolyMem Silver®. *Burns* **40**, 89–96 (2014).

76. Holbrook, R. D., Rykaczewski, K. & Staymates, M. E. Dynamics of silver nanoparticle release from wound dressings revealed via in situ nanoscale imaging. *J. Mater. Sci. Mater. Med.* **25**, 2481–2489 (2014).

77. Dubey, P. *et al.* Silver-nanoparticle incorporated composite nanofibers for potential wound-dressing applications. *J. Appl. Polym. Sci.* **132**, 1–12 (2015).

78. Lu, L. *et al.* Silver nanoparticle/chitosan oligosaccharide/poly(vinyl alcohol) nanofibers as wound dressings: a preclinical study. *Int. J. Nanomedicine* **8**, 4131–4145 (2013).

79. Maneerung, T., Tokura, S. & Rujiravanit, R. Impregnation of silver nanoparticles into bacterial cellulose for antimicrobial wound dressing. *Carbohydr. Polym.* **72**, 43–51 (2008).

80. Xu, Y., Scales, A., Jordan, K., Kim, C. & Sismour, E. Starch nanocomposite films incorporating grape pomace extract and cellulose nanocrystal. *J. Appl. Polym. Sci.* **134**, (2017).

81. McKeen, L. W. Elastomers and Rubbers. in *The Effect of UV Light and Weather on Plastics and Elastomers* 299–370 (Elsevier, 2013). doi:10.1016/B978-1-4557-2851-0.00012-8

82. Wang, S. Styrene-butadiene elastomers. in *Polymer Data Handbook* (ed. Mark, J. E.) 983–986 (Oxford University Press, 1999). doi:10.1021/ja907879q

83. Yip, E. & Cacioli, P. The manufacture of gloves from natural rubber latex. *J. Allergy Clin. Immunol.* **110**, S3–S14 (2002).

84. Mekonnen, T. H., Ah-Leung, T., Hojabr, S. & Berry, R. Investigation of the co-coagulation of natural rubber latex and cellulose nanocrystals aqueous dispersion. *Colloids Surfaces A Physicochem. Eng. Asp.* **583**, 123949 (2019).

85. Favier, V., Dendievel, R., Canova, G., Cavaille, J. Y. & Gilormini, P. Simulation and modeling of three-dimensional percolating structures: case of a latex matrix reinforced by a network of cellulose fibers. *Acta Mater.* **45**, 1557–1565 (1997).

86. Favier, V. *et al.* Nanocomposite materials from latex and cellulose whiskers. *Polym. Adv. Technol.* **6**, 351–355 (1995).

87. Dufresne, A. Nanocellulose: a new ageless bionanomaterial. *Mater. Today* **16**, 220–227 (2013).

88. ASTM Standard E96. Standard Test Methods for Water Vapor Transmission of Materials. *ASTM International* (2000). doi:10.1520/E0096

89. Crank, J. *The Mathematics of Diffusion*. (Oxford University Press, 1975). doi:10.1177/004057368303900411

90. Sobrinho, L. L., Ferreira, M. & Bastian, F. L. The effects of water absorption on an ester vinyl resin system. *Mater. Res.* **12**, 353–361 (2009).

91. Hameed, A. M. & Helal, R. H. The diffusion coefficients of different types of liquid environments into binary polymer blend. *J. Al-Nahrain Univ.* **16**, 148–158 (2013).

92. Nan, C.-W. Physics of inhomogeneous inorganic materials. *Prog. Mater. Sci.* **37**, 1–116 (1993).

93. Crosby, A. J. & Lee, J.-Y. Polymer nanocomposites: the 'nano' effect on mechanical properties. *Polym. Rev.* **47**, 217–229 (2007).

94. Marquis, D. M., Guillaume, É. & Chivas-Joly, C. Properties of nanofillers in polymer. in *Nanocomposites and Polymers with Analytical Methods* 261–284 (2011). doi:10.5772/21694

95. Blanchard, R., Ogunsona, E. O., Hojabr, S., Berry, R. & Mekonnen, T. H. Synergistic cross-linking and reinforcing enhancement of rubber latex with cellulose nanocrystals for glove applications. *ACS Appl. Polym. Mater.* **2**, 887–898 (2020).

96. Bokobza, L. The reinforcement of elastomeric networks by fillers. *Macromol. Mater. Eng.* **289**, 607–621 (2004).

97. Jordan, J., Jacob, K. I., Tannenbaum, R., Sharaf, M. A. & Jasiuk, I. Experimental trends in polymer nanocomposites—a review. *Mater. Sci. Eng. A* **393**, 1–11 (2005).

98. Arencón, D. & Velasco, J. I. Fracture toughness of polypropylene-based particulate composites. *Materials (Basel).* **2**, 2046–2094 (2009).

99. Muiruri, J. K. *et al.* Cavitation-crazing transition in rubber toughening of poly(lactic acid)-cellulose nanocrystal composites. *Compos. Sci. Technol.* **168**, 12–19 (2018).

100. World Health Organization. Antibiotic resistance. Available at: https://www.who.int/news-room/fact-sheets/detail/antibiotic-resistance. (Accessed: 20th July 2020)

101. Bush, K. *et al.* Tackling antibiotic resistance. *Nature Reviews Microbiology* **9**, 894–896 (2011).

102. Canadian Patient Safety Institute. Surgical Site Infection (SSI). Available at: http://www.patientsafetyinstitute.ca/en/Topic/Pages/Surgical-Site-Infection-(SSI).aspx. (Accessed: 7th September 2018)

103. Einav, L., Finkelstein, A. & Mahoney, N. *Long-term care hospitals: a case study in waste*. *National Bureau of Economic Research* **53**, (2018).

104. Arab, M., Safari, H., Zandian, H. & Nodeh, F. H. Evaluation of practicing safety features for hospital waste collection among Iran's public hospitals. *J. Mater. Cycles Waste Manag.* **19**, 939–945 (2017).

105. Hu, Z., Berry, R. M., Pelton, R. & Cranston, E. D. One-pot water-based hydrophobic surface modification of cellulose nanocrystals using plant polyphenols. *ACS Sustain. Chem. Eng.* **5**, 5018–5026 (2017).

106. Mao, H., Liao, Y., Ma, J., Zhao, S. L. & Huo, F. W. Water-soluble metal nanoparticles stabilized by plant polyphenols for improving the catalytic properties in oxidation of alcohols. *Nanoscale* **8**, 1049–1054 (2016).

107. Oza, G. *et al.* Plant-based metal and metal alloy nanoparticle synthesis: a comprehensive mechanistic approach. *J. Mater. Sci.* **55**, 1309–1330 (2020).

108. Iravani, S. Green synthesis of metal nanoparticles using plants. *Green Chem.* **13**, 2638–2650 (2011).

109. Ahmad, T. Reviewing the tannic acid mediated synthesis of metal nanoparticles. *J. Nanotechnol.* **2014**, 1–11 (2014).

110. Ranoszek-Soliwoda, K. *et al.* The role of tannic acid and sodium citrate in the synthesis of silver nanoparticles. *J. Nanoparticle Res.* **19**, 273 (2017).

111. Aswathy Aromal, S. & Philip, D. Facile one-pot synthesis of gold nanoparticles using tannic acid and its application in catalysis. *Phys. E Low-Dimensional Syst. Nanostructures* **44**, 1692–1696 (2012).

112. Tang, H. R., Covington, A. D. & Hancock, R. A. Structure-activity relationships in the hydrophobic interactions of polyphenols with cellulose and collagen. *Biopolymers* **70**, 403–413 (2003).

113. Bensalah, N., Chair, K. & Bedoui, A. Efficient degradation of tannic acid in water by UV/H2O2 process. *Sustain. Environ. Res.* **28**, 1–11 (2018).

114. Martínez-Castañón, G. A., Niño-Martínez, N., Martínez-Gutierrez, F., Martínez-Mendoza, J. R. & Ruiz, F. Synthesis and antibacterial activity of silver nanoparticles with different sizes. *J. Nanoparticle Res.* **10**, 1343–1348 (2008).

115. Erickson, H. P. How bacterial cell division might cheat turgor pressure – a unified mechanism of septal division in Gram-positive and Gram-negative bacteria. *BioEssays* **39**, 1–10 (2017).

116. Slavin, Y. N., Asnis, J., Häfeli, U. O. & Bach, H. Metal nanoparticles: understanding the mechanisms behind antibacterial activity. *J. Nanobiotechnology* **15**, 1–20 (2017).

117. Wei, X., Yang, Z., Wang, Y., Tay, S. L. & Gao, W. Polymer antimicrobial coatings with embedded fine Cu and Cu salt particles. *Appl. Microbiol. Biotechnol.* **98**, 6265–6274 (2014).

118. Tamboli, D. P. & Lee, D. S. Mechanistic antimicrobial approach of extracellularly synthesized silver nanoparticles against gram positive and gram negative bacteria. *J. Hazard. Mater.* **260**, 878–884 (2013).

119. Dizaj, S. M., Lotfipour, F., Barzegar-Jalali, M., Zarrintan, M. H. & Adibkia, K. Antimicrobial activity of the metals and metal oxide nanoparticles. *Materials Science and Engineering C* **44**, 278–284 (2014).

120. Wang, L., Hu, C. & Shao, L. The antimicrobial activity of nanoparticles: present situation and prospects for the future. *Int. J. Nanomedicine* **Volume 12**, 1227–1249 (2017).

121. Bankier, C. *et al.* Synergistic antibacterial effects of metallic nanoparticle combinations. *Sci. Rep.* **9**, 16074 (2019).

122. Rossi, L. M., Fiorio, J. L., Garcia, M. A. S. & Ferraz, C. P. The role and fate of capping ligands in colloidally prepared metal nanoparticle catalysts. *Dalt. Trans.* **47**, 5889–5915 (2018).

123. Mohamad, N., Muchtar, A., Ghazali, M. J., Dahlan, H. M. & Azhari, C. H. Epoxidised natural rubber - alumina nanoparticle composites (ENRAN): effect of filler loading on the tensile properties. *Solid State Sci. Technol.* **17**, 133–143 (2009).

124. Hoy, R. S. & Robbins, M. O. Strain hardening of polymer glasses: effect of entanglement density, temperature, and rate. *J. Polym. Sci. Part B Polym. Phys.* **44**, 3487–3500 (2006).

125. Srivastava, S. & Mishra, Y. Nanocarbon reinforced rubber nanocomposites: detailed insights about mechanical, dynamical mechanical properties, Payne, and Mullin effects. *Nanomaterials* **8**, 945 (2018).

126. Jardin, J. M., Zhang, Z., Hu, G., Tam, K. C. & Mekonnen, T. H. Reinforcement of rubber nanocomposite thin sheets by percolation of pristine cellulose nanocrystals. *Int. J. Biol. Macromol.* **152**, 428–436 (2020).

127. Sivaraman, S. K. & Elango, I. A green protocol for room temperature synthesis of silver nanoparticles in seconds. *Curr. Sci.* **97**, 1055–1059 (2009).